Chapter 7

Localized structures and their stability

In this chapter stability of a single stationary DS is studied. In section 7.1 the results of a linear stability analysis are presented and critical eigenfunctions, which could have an influence on the dynamics of the stationary DS are found. The influence of the mode leading to breathing DSs is discussed in section 7.2 and the amplitude equation for the amplitude of the instable mode is obtained. In section 7.3 travelling DSs are studied and it is shown both theoretically and experimentally that a stationary DS can start to move because of change of its shape. A more complicated situation, when two critical modes become unstable simultaneously is numerically studied in section 7.4. Finally, a long-time dynamics of the DS in the situation that several modes are unstable is briefly discussed in section 7.5.

7.1 General concepts and linear stability analysis

7.1.1 Stationary solutions

In this chapter we concentrate on the behavior of the two-dimensional solitary localized solutions of the three-component RD system

$$\begin{aligned} \partial_t u =& D_u \Delta u + f(u) - \kappa_3 v - \kappa_4 w + \kappa_1, \\ \tau \partial_t v =& D_v \Delta v + u - v, \\ \theta \partial_t w =& D_w \Delta w + u - w. \end{aligned} \tag{7.1}$$

As before $u = u(\mathbf{r}, t)$ is the activating component, whereas $v = v(\mathbf{r}, t)$ and $w = w(\mathbf{r}, t)$ denote the inhibiting components and $\mathbf{r} \subset \mathbb{R}^2$. In the polynomial function $f(u) = \lambda u - u^3$ the coefficient λ is positive. D_u, D_v, D_w denote the (positive) diffusion coefficients of the components, whereas the positive parameters τ and θ represent dimensionless constants, being the ratios of the characteristic times of both inhibitors with respect to the that of the activator. The coefficient κ_1 violates the inversion symmetry ($u \mapsto -u$) and has

arbitrary sign. Finally, the constants κ_3 and κ_4 staying in reaction term are also positive, indicating inhibiting nature of v and w. Let us assume that system (7.1) has a nontrivial stationary solution $\mathbf{u_s} = (u_s, v_s, w_s)^T$. In the simplest case it is a stationary localized structure with rotational symmetry (see Fig. 7.1 (a,b) and corresponding cross-sections Fig. 7.1 (c,d)). Notice that depending on system parameters the asymptotic behavior of the stationary solution can be different. Namely, stationary DS can either decay in space monotonically (Fig. 7.1 (a,c)) towards the ground state or decay in an oscillatory manner (Fig. 7.1 (b,d)). As a rule of thumb one can note that for parameter set closed to that of Turing destabilization, DSs exhibiting oscillatory tails are observed, while otherwise a monotonic decay is to see. Analytical expressions for parameter regions corresponding to monotonic or oscillatory tails behavior are rather simple to obtain for two-component RD system in one and two dimensions, linearizing corresponding system about homogeneous solution and analyzing the corresponding biquadratic equation for eigenvalues [Bode, 1993, Schenk et al., 1998, Purwins et al., 2005]. For the three-component system (7.1) this equation becomes bicubic, what makes the problem more complicated. Nevertheless, this result can be easily obtained numerically for given parameter set.

7.1.2 Linear stability analysis

Let us now discuss stability of the stationary solution $\mathbf{u_s}$. With this object in mind we rewrite the system (7.1) in a more general form:

$$\partial_t \mathbf{u} = \mathfrak{L}\mathbf{u}, \tag{7.2}$$

where in our case $\mathbf{u} = \mathbf{u}(\mathbf{r}, t) = (u, v, w)^T$ is a vector-function, $\mathbf{r} \subset \mathbb{R}^2$, $\mathfrak{L}$ is a real-valued nonlinear operator,

$$\mathfrak{L} = D\Delta + R(\cdot). \tag{7.3}$$

Here Δ denotes the Laplace operator, the diagonal matrix D contains the diffusion constants of u, v, w on the principal diagonal and vector $R(\mathbf{u})$ stands for nonlinear reaction term. We suppose that the system (7.2) has a stationary solution $\mathbf{u_s}$, i.e., $\mathfrak{L}\mathbf{u_s} = 0$ and we are interested in its stability. For this purpose consider a small perturbation $\widetilde{\mathbf{u}}$, so that $\mathbf{u} = \mathbf{u_s} + \widetilde{\mathbf{u}}$. Then the corresponding equation for it takes the form:

$$\partial_t \widetilde{\mathbf{u}} = \mathfrak{L}'(\mathbf{u_s})\widetilde{\mathbf{u}} + \frac{1}{2!}\mathfrak{L}''(\mathbf{u_s})\widetilde{\mathbf{u}}\widetilde{\mathbf{u}} + \frac{1}{3!}\mathfrak{L}'''(\mathbf{u_s})\widetilde{\mathbf{u}}\widetilde{\mathbf{u}}\widetilde{\mathbf{u}} + \cdots, \tag{7.4}$$

where we assume that Tailor expansion of $\mathfrak{L}(\mathbf{u_s} + \widetilde{\mathbf{u}})$ is possible. Here $\mathfrak{L}^{(n)}(\mathbf{u_s})$ denotes n'th Fréchet derivative with respect to $\mathbf{u}$ calculated at $\mathbf{u} = \mathbf{u_s}$. The first coefficient of the expansion (7.4) is the linearization of the operator $\mathfrak{L}$

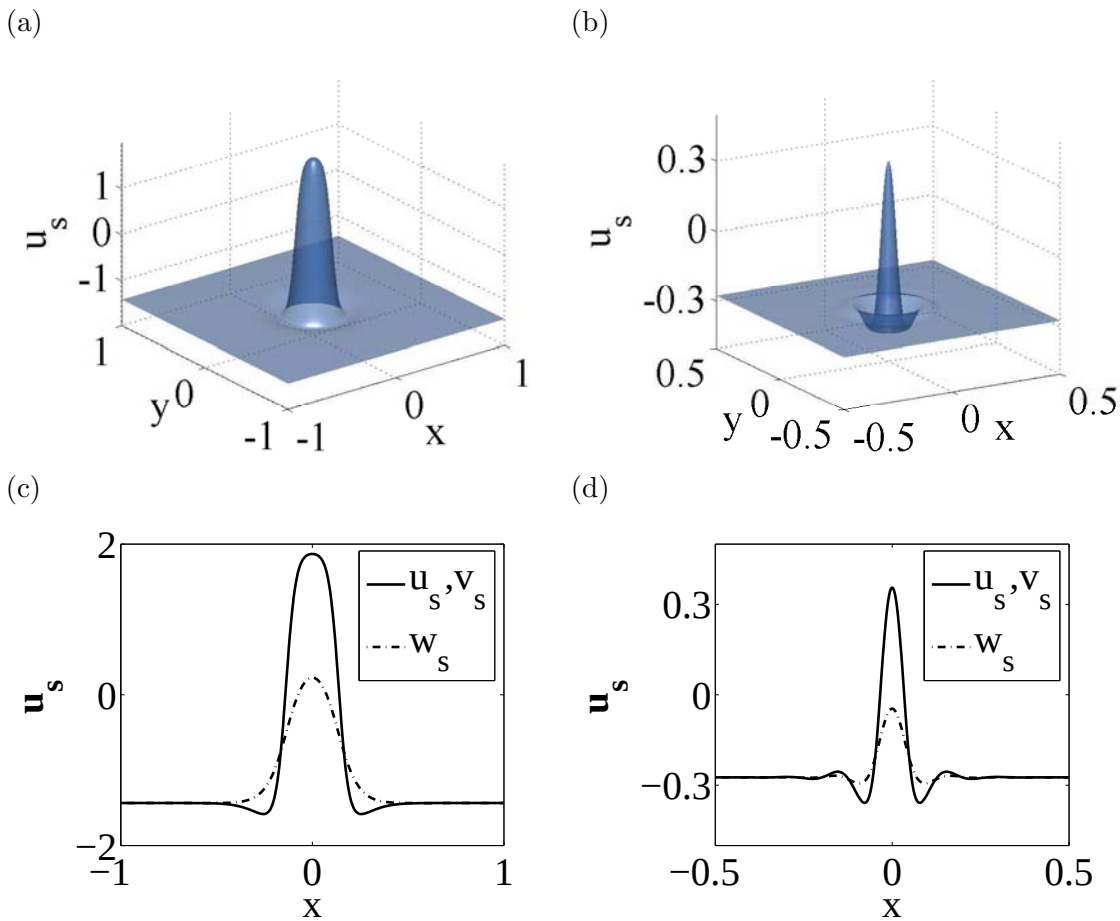

FIG. 7.1: Numerical solution of (7.1) in $\Omega = [-1,1] \times [-1,1] \subset \mathbb{R}^2$ showing stationary activator distribution u_s in the case of (a) monotonic tails; (b) oscillatory tails. The corresponding cross-sections $u_s(x,0)$ for monotonic (c) and oscillatory (d) decay as well as inhibitor distributions $v_s(x,0), w_s(x,0)$ are also to see. Parameters: (a,c) $D_u = 4.7 \cdot 10^{-3}$, $D_v = 0$, $D_w = 0.01$, $\lambda = 5.67$, $\kappa_1 = -1.04$, $\kappa_3 = 1$, $\kappa_4 = 3.33$; (b,d) $D_u = 1.1 \cdot 10^{-4}$, $D_v = 0$, $D_w = 9.64 \cdot 10^{-4}$, $\lambda = 1.01$, $\kappa_1 = -0.1$, $\kappa_3 = 0.3$, $\kappa_4 = 1$. Boundary conditions in both cases are Neumann.

around the stationary solution $\mathbf{u_s}$, the second term corresponds to the bilinear operator, acting on two perturbation vectors $\widetilde{\mathbf{u}}$, etc.

First we take a detailed look at the linear equation

$$\partial_t \widetilde{\mathbf{u}} = \mathfrak{L}'(\mathbf{u_s})\widetilde{\mathbf{u}}$$

and discuss key properties and features of the linear operator $\mathfrak{L}'(\mathbf{u_s})$. To this end we briefly review some notations, which will be used hereinafter.

Let $L^2(\Omega)$, $\Omega \subset \mathbb{R}^n$, be a Hilbert space of square integrable functions. We assume that all solutions of interest are localized and belong to this space. Then one can define a scalar product $\langle\cdot|\cdot\rangle$ of two arbitrary complex-valued vector-functions $\mathbf{u}(\mathbf{r},t) = (u_1,\ldots,u_m)^T$ and $\mathbf{v}(\mathbf{r},t) = (v_1,\ldots,v_m)^T$ by standard convention:

$$\langle \mathbf{u}|\mathbf{v}\rangle = \int d^n\mathbf{r} \sum_{k=1}^{m} u_k \bar{v}_k, \tag{7.5}$$

where overline stands for a complex conjugation. Notice, that in this definition of the scalar product the first factor is taken linear whereas the second one–semilinear, as is usual in mathematics and not conversely, as is usual in physics. In particular, it implies that for some scalar quantity a equality $\langle \mathbf{u}|a\mathbf{v}\rangle = \bar{a}\langle \mathbf{u}|\mathbf{v}\rangle$ is fulfilled.

Keeping in mind definition (7.5) one can define *an adjoint* operator $\mathfrak{L}'^{\dagger}(\mathbf{u_s})$ to the linear operator $\mathfrak{L}'(\mathbf{u_s})$ as one with the following property

$$\langle \mathbf{u}|\mathfrak{L}'(\mathbf{u_s})\mathbf{v}\rangle = \langle \mathfrak{L}'^{\dagger}(\mathbf{u_s})\mathbf{u}|\mathbf{v}\rangle.$$

As can be easily shown for the system (7.1) the operator $\mathfrak{L}'(\mathbf{u_s})$ is not *Hermitian* (or *symmetrical*), i.e., $\mathfrak{L}'^{\dagger}(\mathbf{u_s}) \neq \mathfrak{L}'(\mathbf{u_s})$. It implies that if we consider the eigenvalue problem

$$\mathfrak{L}'(\mathbf{u_s})\mathcal{F} = \lambda\mathcal{F}, \tag{7.6}$$

the eigenvalues λ and corresponding eigenfunctions (modes) $\mathcal{F}$ are in general complex.

The linear stability of $\mathbf{u_s}$ implies that all eigenvalues of (7.6) have negative real parts. If the real part of one or more eigenvalues is equal to zero one speaks about *neutral stability* of the system. As the system (7.1) features translational invariance with respect to its spatial coordinates, $\lambda = 0$ is an eigenvalue of the operator $\mathfrak{L}'(\mathbf{u_s})$, corresponding to two independent neutral eigenfunctions (one for each spatial direction), which in the following will be called *Goldstone modes*. This statement becomes clear when keeping in mind that in systems possessing translational invariance, each solution of the system remains a solution if it is shifted to a different spatial position; a small perturbation of $\mathbf{u_s}$ in the form of Goldstone mode is equivalent to the shift of the stationary solution in the respective direction,

$$\mathbf{u_s}(\mathbf{r}+\epsilon) = \mathbf{u_s}(\mathbf{r}) + \epsilon\frac{\partial \mathbf{u_s}}{\partial \mathbf{r}} + O(\epsilon^2).$$

As an infinitesimal shift corresponds to an addition of the spatial derivative of the solution in the respective direction, the Goldstone modes can be identified as the first derivatives of $\mathbf{u_s}$ with respect to $\mathbf{r}$, where $\mathbf{r} = x, y$ are the spatial coordinates, i.e.,

$$\mathcal{G}_{\mathbf{r}} = \partial \mathbf{u_s} / \partial \mathbf{r}.$$

As we mentioned before, the linear stability of the DS implies that the real parts of all eigenvalues of (7.6) but $\lambda = 0$ have negative real parts. Therefore a slight disturbance of $\mathbf{u_s}$ in the form of $\mathcal{G}_{\mathbf{r}}$, causes only a translation of the stationary solution, its stability is not affected.

In the case of reaction-diffusion systems one can speak about *a compact* operator $\mathfrak{L}'(\mathbf{u_s})$, namely the operator, whose *continuous* spectrum is separated from zero. That is, only a finite number of modes, whose eigenvalues are situated near to zero and belong to *the discrete* spectrum can become unstable by the change of the control parameter. These modes are also often called *critical* [Haken, 1983].

In order to find these critical modes for a given parameter set one should solve the eigenvalue problem (7.6). For this purpose one can rewrite the system (7.1) in polar coordinates, decompose the small perturbation $\widetilde{\mathbf{u}}$ of the radially symmetric stationary solution $\mathbf{u_s}$ into a Fourier series and finally rewrite the eigenvalue problem (7.6) in terms of the amplitude $\widetilde{\mathbf{u}}_n$ of the perturbation of the stationary solution with angular dependence $e^{in\varphi}$,

$$\lambda_n \widetilde{\mathbf{u}}_n = \mathfrak{L}'_p \widetilde{\mathbf{u}}_n,$$

where $\mathfrak{L}'_p$ denotes the linearization operator $\mathfrak{L}'$ in polar coordinates,

$$\mathfrak{L}'_p = D(\partial_{rr} + \frac{1}{r}\partial_r - \frac{n^2}{r^2}) + R(\cdot).$$

Then the influence of the modes with different n on the radial-symmetrical DS can be understood as follows: the mode with $n = 0$ (breathing mode) results in the change of the size of the DS; the mode with $n = 1$ (Goldstone mode $\mathcal{G}$) describes the shift of the solution and $n \geq 2$ leads to different deformations of the DS [Schenk, 1999]. An example of real parts of first four critical modes belonging to the discrete spectrum is shown in Fig. 7.2 (for the mode $n = 1$ the corresponding eigenfunction is real).

As mentioned before, the stationary DS $\mathbf{u_s}$ can loose its stability with the change of one or more control parameters. In what follows, we use the time constants τ and θ as control parameters. This is convenient because the stationary solution does not depend on them. Now we can solve the eigenvalue problem (7.6) numerically for different values of the control parameters τ and θ, keeping all other parameters fixed. The stability diagram and the graphic illustration of the influence of the modes $n = 0$ and $n = 1$ on the radial-symmetrical object can be seen in Fig. 7.3. One can easily see that for small

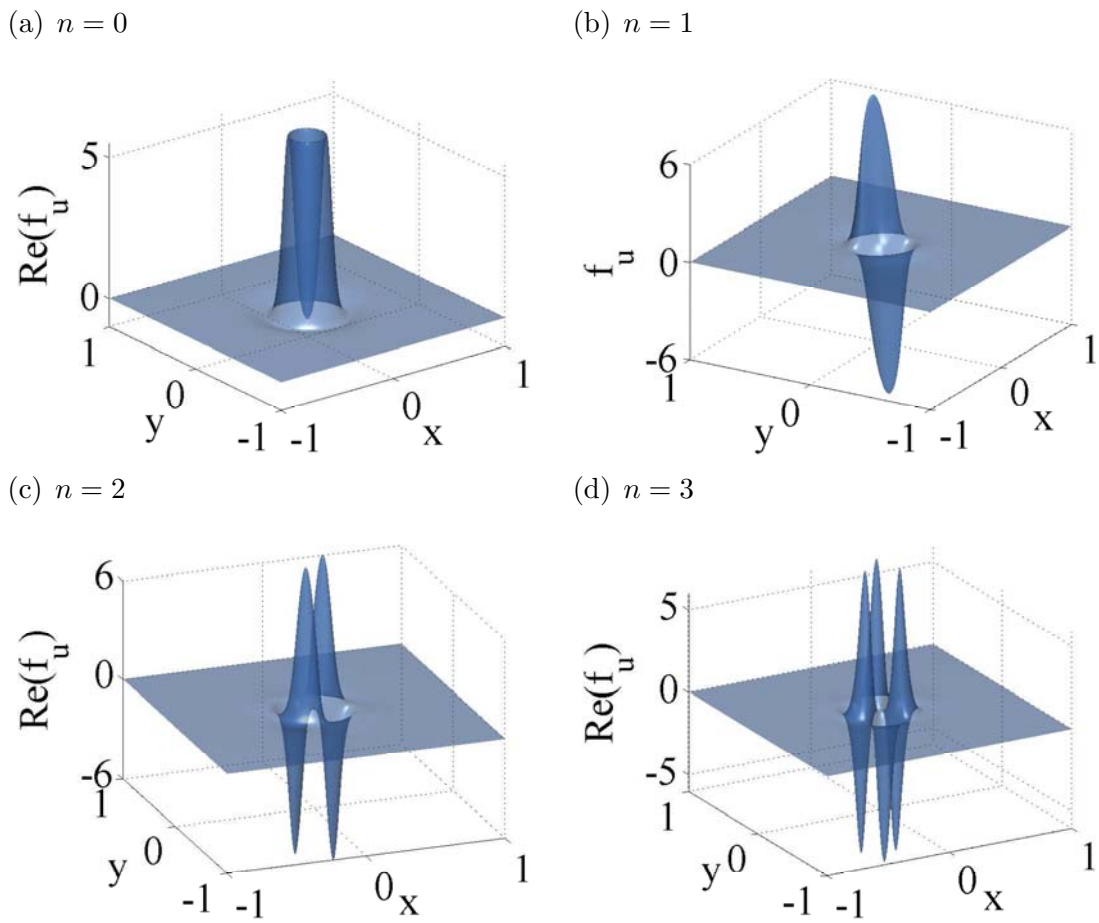

FIG. 7.2: Real parts of first four eigenfunctions of (7.6), corresponding to different n. The real parts of the first component of $\mathcal{F} = (f_u, f_v, f_w)$ are shown. (a) breathing mode $n = 0$; (b) Goldstone mode $n = 1$; (c)(d) $n = 2, 3$ – modes, responsible for different deformations of DS.

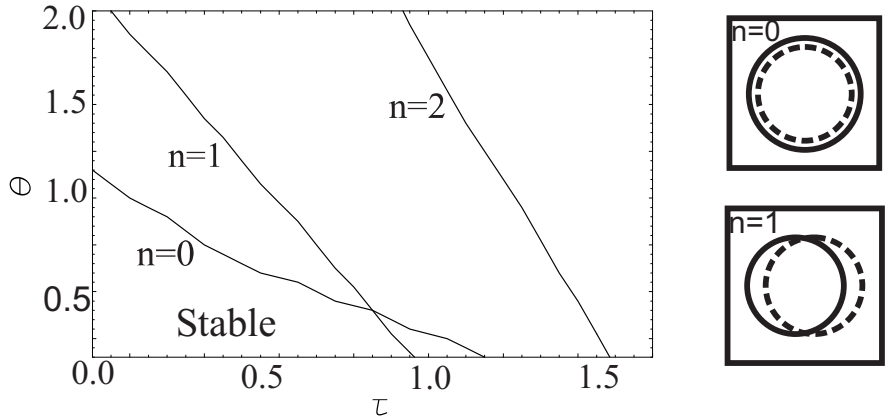

FIG. 7.3: Stability diagram in (τ, θ) plane, calculated for a solitary solution of the system (7.1). Lines separate stability regions, corresponding to different modes n=0,1,2. Parameters: $D_u = 4.7 \cdot 10^{-3}$, $D_v = 0$, $D_w = 0.01$, $\lambda = 5.67$, $\kappa_1 = -1.04$, $\kappa_3 = 1.0$, $\kappa_4 = 3.33$. On the right-hand side the dotted line shows the influence of a breathing mode $n = 0$ and a drift mode $n = 1$ on a rotation-symmetrical object, depicted by the solid line.

values of τ and θ the stationary solution is stable. An increase of the constants leads to the excitation of either $n = 0$ or $n = 1$ mode. Notice that for the chosen parameter set the breathing mode $n = 0$ becomes unstable first for all θ but $\theta = 0$. The latter situation was investigated in, e.g., [Or-Guil et al., 1998] and leads to the drift-bifurcation of DSs. The modes $n \geq 2$ become unstable for larger value of τ and θ and cannot be responsible for the primary destabilizaion. So the primary destabilization of stationary DS for presented control parameter values can be caused only by the modes $n = 0$ and $n = 1$. The influence of these modes on the stationary DS will be considered in the following sections.

7.1.3 Properties of the operator $\mathfrak{L}'(\mathbf{u_s})$ and its spectrum

In order to investigate the influence of the modes $n = 0$ and $n = 1$ on the stationary DS, let us first briefly discuss some properties of the linearization operator $\mathfrak{L}'(\mathbf{u_s})$ and its spectrum. As we mentioned before, the linearization operator $\mathfrak{L}'(\mathbf{u_s})$ is not Hermitian. Nevertheless it can be represented as a product [Moskalenko et al., 2003, Gurevich et al., 2004b]

$$\mathfrak{L}'(\mathbf{u_s}) = ML(\mathbf{u_s}), \tag{7.7}$$

of an invertible matrix

$$M = \begin{pmatrix} 1 & 0 & 0 \\ 0 & -1/\kappa_3\tau & 0 \\ 0 & 0 & -1/\kappa_4\theta \end{pmatrix}$$

and a Hermitian operator

$$L = \begin{pmatrix} D_u\triangle + \lambda - 3\bar{u}^2 & -\kappa_3 & -\kappa_4 \\ -\kappa_3 & -\kappa_3 D_v\triangle + \kappa_3 & 0 \\ -\kappa_4 & 0 & -\kappa_4 D_w\triangle + \kappa_4 \end{pmatrix}.$$

The class of operators, represented by the product of two Hermitian operators occurs widely in different physical problems, e.g., in the stability problem for the solitons in nonlinear Schrödinger equation (NSE) [Zakharov et al., 1986]. Nevertheless to best of our knowledge it has no special name. The properties of these operators depend on the fact whether the matrix (or operator) M is positive definite or not. In the former case determining a new scalar product (7.5) as

$$(\mathbf{u}|\mathbf{v}) := \langle M^{-1}\mathbf{u}|\mathbf{v}\rangle, \tag{7.8}$$

one can easily verify that the operator $\mathfrak{L}'(\mathbf{u_s})$ becomes Hermitian with respect to the new scalar product (7.8) and therefore has a relatively simple structure. On the other hand, in our case the matrix M is not positive definite, therefore the operator $\mathfrak{L}'(\mathbf{u_s})$ being a composition of two Hermitian operators, is not Hermitian, so its spectrum is complex, one can expect Jordan chains, etc.

Let us now look for possible connections between the spectrums of the operator $\mathfrak{L}'(\mathbf{u_s})$ and its adjoint operator $\mathfrak{L}'^{\dagger}(\mathbf{u_s})$. In general, it is known that if λ is an eigenvalue of $\mathfrak{L}'(\mathbf{u_s})$, its complex conjugated $\bar{\lambda}$ is an eigenvalue of $\mathfrak{L}'^{\dagger}(\mathbf{u_s})$. Nevertheless in general no relation between the corresponding eigenfunctions, say $\mathcal{F}$ and $\mathcal{F}^*$ can be established. In our case, however, such a relation does exist. To find it, consider two eigenvalue problems for these operators:

$$\begin{aligned} \mathfrak{L}'(\mathbf{u_s})\mathcal{F} &= \lambda\mathcal{F}, \qquad & \mathfrak{L}'^{\dagger}(\mathbf{u_s})\mathcal{F}^* &= \bar{\lambda}\mathcal{F}^*, \\ \mathfrak{L}'(\mathbf{u_s})\overline{\mathcal{F}} &= \bar{\lambda}\overline{\mathcal{F}}, \qquad & \mathfrak{L}'^{\dagger}(\mathbf{u_s})\overline{\mathcal{F}}^* &= \lambda\overline{\mathcal{F}}^*. \end{aligned} \tag{7.9}$$

Here $\mathcal{F}$ and $\overline{\mathcal{F}}$ denotes the eigenfunctions of the operator $\mathfrak{L}'(\mathbf{u_s})$, corresponding to the eigenvalues λ and $\bar{\lambda}$, whereas $\mathcal{F}^*$ and $\overline{\mathcal{F}}^*$ denote the eigenfunctions of the adjoint operator, corresponding to the eigenvalues $\bar{\lambda}$ and λ and overline stands for the complex conjugation.

Statement. *Let $\mathcal{F}$ be an eigenfunction of the operator $\mathfrak{L}'(\mathbf{u_s})$ corresponding to the complex eigenvalue λ and $\mathcal{F}^*$ be an eigenfunction of $\bar{\lambda}$. Then $\mathcal{F}$ is orthogonal to the eigenvector $\overline{\mathcal{F}}^*$ of the adjoint operator $\mathfrak{L}'^{\dagger}(\mathbf{u_s})$, corresponding to the same complex eigenvalue λ. Moreover, the eigenfunctions $\mathcal{F}$ and $\overline{\mathcal{F}}^*$ are related by formula*

$$\overline{\mathcal{F}}^* = M^{-1}\mathcal{F}. \tag{7.10}$$

Indeed, according to (7.9), $\langle\mathfrak{L}'^{\dagger}(\mathbf{u_s})\overline{\mathcal{F}}^*|\mathcal{F}\rangle = \lambda\langle\overline{\mathcal{F}}^*|\mathcal{F}\rangle$. On the other hand, by the definition of the adjoint operator,

$$\langle\mathfrak{L}'^{\dagger}(\mathbf{u_s})\overline{\mathcal{F}}^*|\mathcal{F}\rangle = \langle\overline{\mathcal{F}}^*|\mathfrak{L}'(\mathbf{u_0})\mathcal{F}\rangle = \bar{\lambda}\langle\overline{\mathcal{F}}^*|\mathcal{F}\rangle.$$

Hence, from two last equations we get

$$(\lambda - \bar{\lambda})\langle \overline{\mathcal{F}}^* | \mathcal{F} \rangle = 0,$$

and therefore if λ is not real $\langle \overline{\mathcal{F}}^* | \mathcal{F} \rangle = 0$. Now let us show that $\overline{\mathcal{F}}^* = M^{-1}\mathcal{F}$. Indeed, by definition (7.9)

$$\mathfrak{L}'^{\dagger}(\mathbf{u_s})\overline{\mathcal{F}}^* = \lambda \overline{\mathcal{F}}^* \Leftrightarrow L \underbrace{MM^{-1}}_{E} \mathcal{F} = \lambda M^{-1}\mathcal{F} \Leftrightarrow \underbrace{ML}_{\mathfrak{L}'(\mathbf{u_s})} \mathcal{F} = \lambda \mathcal{F} \Leftrightarrow \mathfrak{L}'(\mathbf{u_s})\mathcal{F} = \lambda \mathcal{F},$$

as it should be (see (7.9)).

Notice that the expression (7.10) is also correct, even if λ is real. For instance, let $\mathcal{G}_r^*$ be the eigenfunctions of the adjoint operator, corresponding to the zero eigenvalue. Then

$$\mathcal{G}_r^* = M^{-1}\mathcal{G} = \begin{pmatrix} \frac{\partial \mathbf{u_s}}{\partial \mathbf{r}} \\ -\kappa_3 \tau \frac{\partial \mathbf{v_s}}{\partial \mathbf{r}} \\ -\kappa_4 \theta \frac{\partial \mathbf{w_s}}{\partial \mathbf{r}} \end{pmatrix}. \tag{7.11}$$

However, in this case $\langle \mathcal{G}_r^* | \mathcal{G} \rangle \neq 0$.

Remark: In a similar way one can show, that $\langle \mathcal{F}^* | \overline{\mathcal{F}} \rangle = 0$ and $\mathcal{F}^* = M^{-1}\overline{\mathcal{F}}$.

The possibility to find the eigenfunctions $\mathcal{F}^*$ (especially $\mathcal{G}_r^*$) explicitly considerably simplifies many problems we face below.

7.2 Destabilization via the mode $n = 0$: Breathing DSs

7.2.1 Breathing DSs

In this section we investigate the influence of the mode $n = 0$ on the dynamic of the stationary DS $\mathbf{u_s}$ by the change of the control parameters. For the sake of simplicity we fix one control parameter, e.g., τ and change only θ. The instability scenario we are interested in is that the pair of a complex-conjugated eigenvalues passes through the imaginary axis as one gradually increases the control parameter. The typical eigenvalues behavior in this case is shown in Fig. 7.4. Here the eigenvalues, corresponding to different eigenfunctions are colored in different ways. The accordingly colored arrows show the "motion" of the eigenvalues on the complex plane by the change of θ. One can see that at the beginning all eigenvalues are situated on left hand side of the plane. By the change of θ all eigenvalues, but $\lambda = 0$ (the corresponding eigenmode $n = 1$ is black colored) start to move as shown by arrows. Notice that the "velocities" of the eigenvalues motion are different. The eigenvalue with largest motion velocity (blue colored eigenvalue, corresponding to $n = 0$) goes into the complex plane and crosses the axis $\mathrm{Im}(\lambda)$ first (see Fig. 7.4).

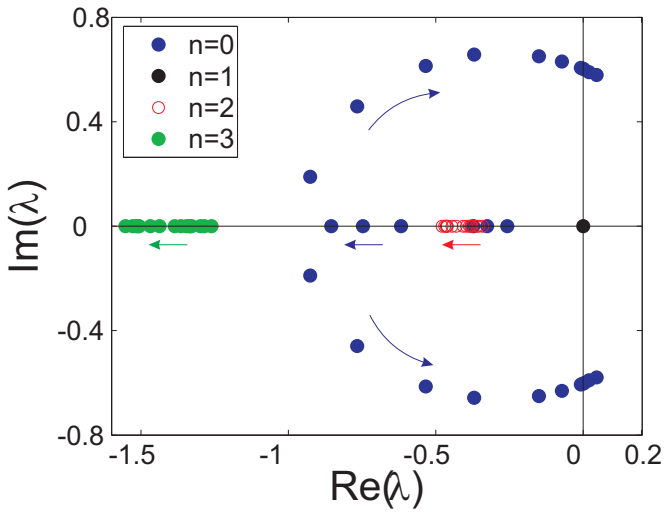

FIG. 7.4: Behaviors of the first four on the complex plane (Re(λ), Im(λ)) by the change of θ in case that the mode $n = 0$ becomes excited first. The eigenvalues corresponding to different eigenfunctions differ in colors (see the legend). The accordingly colored arrows show the "motion" direction of the eigenvalues on the λ plane as θ increases.

Figure 7.5 shows scenarios of the behavior of an initial pulse closed to a stationary DS for different control parameters values, as observed in numerical simulation of the system (7.1). In Fig. 7.5 (a) a stationary DS is stable for given τ and θ, i.e., after some transients the initial distribution converges to an stationary DS, which is numerically stable on a long time scale. Figure 7.5 (b) shows the behavior of the solution just after the mode $n = 0$ becomes excited: a stationary DS bifurcates to an oscillatory DS. The amplitude of oscillations is built up and achieves some constant value, so that the DS oscillates with a constant amplitude on a long time scale. We refer to this oscillating with the constant amplitude soliton as *breathing DS*. Figure 7.5 (c) shows another possible instability scenario. The stationary DS bifurcates to an unstable oscillatory DS with increasing amplitude, in this case it eventually leads to a collapse of the solution. Now, we turn to breathing DSs, the main topic of this section.

Breathing solutions in dissipative systems have attracted a great deal of attention in recent years. They have been found, e.g., as soliton pulsation in fiber laser [Soto-Crespo et al., 2004, Tsoy and Akhmediev, 2005], as rocking localized current filaments in p-n-p-n devices [Niedernostheide et al., 1992c, Niedernostheide et al., 1993] and as breathing spots in chemical reactor [Haim et al., 1996]. Analytical investigations of breathing localized structures in one spatial dimension have been carried out for two-component reaction-diffusion system with piecewise linear activator nullcline [Koga and

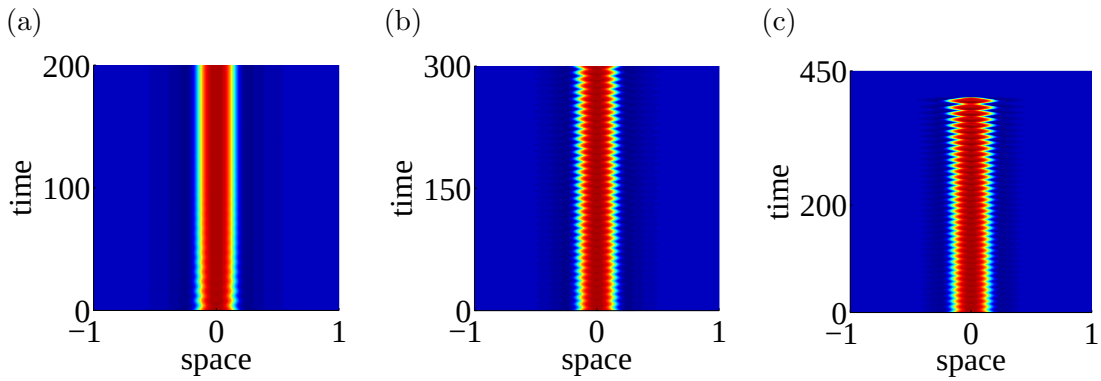

FIG. 7.5: Space-time plots of numerical solution of (7.1). Time evolution of the cross-section of the initial pulse close to the stationary solution is shown; a) $\tau = 0.5$, $\theta = 0.63$, DS is stable; b) $\tau = 0.5$, $\theta = 0.64$, amplitude of oscillations reaches a constant value; c) $\tau = 0.01$, $\theta = 1.22$, increase of the control parameter beyond the critical value leads to the collapse of the soliton. Other parameters: $D_u = 4.7 \cdot 10^{-3}$, $D_v = 0$, $D_w = 0.01$, $\lambda = 5.67$, $\kappa_1 = -1.04$, $\kappa_3 = 1.0$, $\kappa_4 = 3.33$. The calculations was performed on the rectangular domain $\Omega = [-1, 1] \times [-1, 1]$ on nonuniform triangular grid with maximal element size 0.1 with Neumann boundary conditions.

Kuramoto, 1980, Nishiura and Mimura, 1989]. Numerical studies of breathing domains in an infinite medium in two-component system with a cubic nonlinearity also in one-spatial dimension have been performed in [Hagberg and Meron, 1994b]. In the latter study a single stationary domain loses stability via a Hopf bifurcation, and a breathing-like oscillatory motion sets in; as the control parameter is changed further the amplitude of the oscillation grows, thereby leading to the collapse of the domain. Breathing and wiggling motion of layers in reaction-diffusion system with multiple components in one dimension was investigated in [Suzuki et al., 1995]. Quasi-two-dimensional breathing spots have been found experimentally in a disk-shaped chemical reactor [Haim et al., 1996]. In these experiments similar to the theoretical investigation [Hagberg and Meron, 1994b], a circular spot bifurcates to an oscillatory spot when the control parameter is increased beyond some critical value. Further increase of the latter leads to the collapse of the spot. However, these oscillations have been interpreted as an interaction of a front with the system's boundary and not as oscillations of the radius of the spot. Recently, localized breathers have been found in one- and two-dimensional neural media [Bressloff et al., 2003,Folias and Bressloff, 2005], described by a two-component system with an integral term. In particular, in two-dimensional excitable neural media the nonlocal inhibition leads to a symmetry breaking instability of the stationary pulse, resulting in a formation of a non-radially symmetric breather. In addition, the number of breathing lobes corresponds to the dominant unstable Fourier mode associated with perturbations of the stationary solution.

The name breather as such arose from studies of the sine-Gordone (SG)

equation and can be considered as a bound state of its kink and antikink solutions, which oscillate with respect to each other. An important class of breathers is the so-called discrete breathers (or localized modes) [Kivshar and Flach, 2003]. These can be considered as solutions of a nonlinear equation on a lattice and they are periodic in time and localized in space. Localized breathers are found theoretically as well as experimentally in various physical systems where the space discreetness arises in a natural way, e.g., photonic crystals [Mingaleev and Kivshar1, 2001], Josephson junction [Trias et al., 2000] or Bose-Einstein condensates in periodic optical traps [Trombettoni and Smerzi, 2001]. Discrete breathers are observed in conservative and dissipative systems in one- and two spatial dimension.

Another interesting type of localized oscillating solutions are oscillons. An oscillon essentially is a name given to a stable, two-dimensional localized excitations occurring in a vibrating layer of sand [Umbanhowar et al., 1996]. Typically these localized circular regions oscillate between conical peaks and craters with a period of half of the external driving frequency and exist in a narrow region between the stability regions of spatially extended patterns and the ground state. Oscillons were also found in dissipative fluids and colloidal suspensions [Lioubashevski et al., 1999]. Localized oscillons in autonomous chemical system can also be found [Vanag and Epstein, 2004]. However, these localized objects are result of a interaction of subcritical Turing and Hopf instabilities. In contrast to breathers, an external forcing is needed to produce an oscillon (in the case of autonomous systems, subcritical Hopf bifurcation plays such a role, possessing simultaneously a stationary steady state and stable limit cycle.

Here we investigate the transition from stationary to breathing DSs in three-component reaction-diffusion system with one activator and two inhibitors. In contrast to the reaction-diffusion models, mentioned above, where either piecewise linear nullclines or one-dimensional domains were studied, we consider the case of two spatial dimension and a nonlinear reaction term (see also [Gurevich et al., 2006]).

7.2.2 Amplitude equation in general form

Let us remind that we deal with a reaction-diffusion system in general form (7.2) with the nonlinear real-valued operator $\mathfrak{L}$ that depends on some control parameter p and suppose that (7.2) has a stationary solution $\mathbf{u_s}$, which is stable in certain parameter region. The destabilization scenario we are interested in is that pair of a complex-conjugated eigenvalues passes through the imaginary axis as one gradually changes the control parameter p. That is, for some critical value $p = p_c$ the corresponding eigenvalues are purely imaginary, i.e., $\lambda_c = \pm i\omega$. In this case the real-valued perturbation vector-function $\widetilde{\mathbf{u}}$ can

be represented as:

$$\widetilde{\mathbf{u}} = Ae^{i\omega t}\mathcal{F}_c + c.c. + r, \tag{7.12}$$

where $\mathcal{F}_c$ is the eigenfunction of the operator $\mathfrak{L}'(\mathbf{u_s})|_{p=p_c} := \mathfrak{L}'_c$, corresponding to the λ_c. Further, A is a constant oscillation amplitude and r represents the sum of the other decaying modes. Now, if we increase the control parameter $p = p_c + \varepsilon$, where ε is positive and $\varepsilon \ll 1$, the corresponding change of the factor $e^{\lambda t}$ can be "included" in A and the amplitude A becomes a slow function of time, i.e.,

$$\widetilde{\mathbf{u}} = A(t)e^{i\omega t}(\mathcal{F}_c + \varepsilon\mathcal{F}_\varepsilon) + c.c. + r, \tag{7.13}$$

where $\partial_t A \sim \varepsilon A$. Here $\varepsilon\mathcal{F}_\varepsilon$ represents a deviation of the eigenfunction $\mathcal{F}$ from $\mathcal{F}_c$. Our goal now is to write down the ordinary differential equation for the complex amplitude $A(t)$. For this purpose we substitute Eq. (7.13) into Eq. (7.4), equalize the terms with the same frequency and obtain

$$\varepsilon A(\mathfrak{L}'_c(\mathbf{u_s}) - i\omega)\mathcal{F}_\varepsilon = -\partial_t A\mathcal{F}_c + \varepsilon A\mathfrak{L}'_\varepsilon(\mathbf{u_s})\mathcal{F}_c + \frac{1}{2}A^2\bar{A}\mathfrak{L}'''_c(\mathbf{u_s})\mathcal{F}_c\mathcal{F}_c\overline{\mathcal{F}}_c, \tag{7.14}$$

where $\mathfrak{L}'_\varepsilon(\mathbf{u_s}) = \frac{\partial\mathfrak{L}'(\mathbf{u_s})}{\partial p}\Big|_{p=p_c}$ represents the deviation of the operator $\mathfrak{L}'(\mathbf{u_s})$ from the $\mathfrak{L}'_c$, so that

$$\mathfrak{L}'(\mathbf{u_s})|_{p=p_c+\varepsilon} = \mathfrak{L}'_c + \varepsilon\mathfrak{L}'_\varepsilon + O(\varepsilon^2).$$

Equation (7.14) can be interpreted as an equation with respect to the unknown vector-function $\mathcal{F}_\varepsilon$. In accordance with Fredholm alternative this equation is solvable if and only if the right-hand side of Eq. (7.14) is orthogonal to the kernel of the operator, adjoined to the $\mathfrak{L}'_c(\mathbf{u_s}) - i\omega$. This kernel can be easily found and is represented by the eigenfunction $\mathcal{F}^*_c$ of the adjoint operator $\mathfrak{L}'^{\dagger}_c$, corresponding to the eigenvalue $-i\omega$. Indeed, one has to find a nontrivial vector-function $\mathcal{X}$, such that

$$\langle\mathcal{X}|(\mathfrak{L}'_c(\mathbf{u_s}) - i\omega)\mathcal{F}_\varepsilon\rangle = 0.$$

By the definition of the adjoint operator the latter equality is equivalent

$$\langle\mathcal{X}|(\mathfrak{L}'_c(\mathbf{u_s})-i\omega)\mathcal{F}_\varepsilon\rangle = \langle(\mathfrak{L}'^{\dagger}_c(\mathbf{u_s})+i\omega)\mathcal{X}|\mathcal{F}_\varepsilon\rangle = 0 \Leftrightarrow \mathfrak{L}'^{\dagger}_c(\mathbf{u_s})\mathcal{X} = -i\omega\mathcal{X} \Leftrightarrow \mathcal{X} \equiv \mathcal{F}^*_c.$$

After projection Eq. (7.14) onto $\mathcal{F}^*_c$ we get

$$\dot{\bar{A}}\langle\mathcal{F}_c|\mathcal{F}^*_c\rangle = \varepsilon\langle\mathcal{F}^*_c|\mathfrak{L}'_\varepsilon(\mathbf{u_s})\mathcal{F}_c\rangle + \bar{A}^2A\langle\mathcal{F}^*_c|\frac{\mathfrak{L}'''_c(\mathbf{u_s})}{2}\mathcal{F}_c\mathcal{F}_c\overline{\mathcal{F}}_c\rangle.$$

Conjugating the last equation one finally obtains the following equation for the complex amplitude $A(t)$

$$\partial_t A = \varepsilon a_1 A + a_2 A|A|^2, \tag{7.15}$$

which can be recognized as a normal form of a Hopf bifurcation [Kuramoto, 1984]. The coefficients a_1 and a_2 are complex and can be expressed as

$$a_1 = \frac{\langle \mathfrak{L}'_\varepsilon(\mathbf{u_s})\mathcal{F}_c|\mathcal{F}_c^*\rangle}{\langle \mathcal{F}_c|\mathcal{F}_c^*\rangle}, \qquad a_2 = \frac{\langle \mathfrak{L}'''_c(\mathbf{u_s})\mathcal{F}_c\mathcal{F}_c\overline{\mathcal{F}}_c|\mathcal{F}_c^*\rangle}{2\langle \mathcal{F}_c|\mathcal{F}_c^*\rangle}. \tag{7.16}$$

Equation (7.15) has a trivial solution $A = 0$, which for $\mathrm{Re}(a_1) < 0$ is a stable focus. If now $\mathrm{Re}(a_1)$ increases and passes through zero the trivial solution becomes unstable. For $\mathrm{Re}(a_1) > 0$ one can also find the non-trivial periodic solution $A_0(t) = Re^{i\nu t}$, where

$$R = \sqrt{-\varepsilon\frac{\mathrm{Re}(a_1)}{\mathrm{Re}(a_2)}}, \qquad \nu = \varepsilon\mathrm{Im}(a_1) + R^2\mathrm{Im}(a_2).$$

Linearization of Eq. (7.15) about A_0 shows that the periodic solution is stable for $\mathrm{Re}(a_2) < 0$ and unstable, if $\mathrm{Re}(a_2) > 0$. In the former case the instability is stabilized by a limit cycle (nonlinear stabilization) that corresponds to supercritical bifurcation. In the latter case ($\mathrm{Re}(a_2) > 0$) no stabilization takes place and bifurcation is subcritical [Kuramoto, 1984, Tabor, 1989]).

An additional point to emphasize is that the amplitude equation, derived in a similar situation for a steady state solution of a set of ordinary differential equation, e.g., in [Kuramoto, 1984], contains in its nonlinear part contributions from the second harmonics, which are absent in the Eq. (7.15). To find this correction on should rewrite the Eq. (7.12) as

$$\widetilde{\mathbf{u}} = Ae^{i\omega t}\mathcal{F}_c + \mathcal{Y}e^{2i\omega t} + c.c. + r,$$

where $\mathcal{Y}$ is unknown. Substituting the last equation in (7.4) and equalizing the terms with the frequency $2i\omega$ one obtains

$$2i\omega\mathcal{Y} = \mathfrak{L}'(\mathbf{u_s})\mathcal{Y} + \frac{\mathfrak{L}''(\mathbf{u_s})}{2}\mathcal{F}_c\mathcal{F}_cA^2.$$

If $\mathfrak{L}'(\mathbf{u_s})$ can be presented as a matrix one can easily obtain $\mathcal{Y}$. In our case, however, one needs to invert the differential operator $\mathfrak{L}'(\mathbf{u_s})$ explicitly, that usually is not possible. Therefore we estimated this correction for Eqs. (7.1). Assuming it to be proportional to $\mathcal{F}_c$,

$$\widetilde{\mathbf{u}} = Ae^{i\omega t}\mathcal{F}_c + Be^{2i\omega t}\mathcal{F}_c + c.c. + r,$$

one can find B as

$$B = \frac{A^2}{2i\omega}\frac{\langle \mathfrak{L}''(\mathbf{u_s})\mathcal{F}_c\mathcal{F}_c|\mathcal{F}_c^*\rangle}{\langle \mathcal{F}_c|\mathcal{F}_c^*\rangle}.$$

Then the amplitude equation with regard to the contributions from the second harmonics has a form

$$\dot{A} = \varepsilon a_1 A + \left(a_2 + \frac{\langle \mathfrak{L}''(\mathbf{u_s})\mathcal{F}_c\overline{\mathcal{F}}_c|\mathcal{F}_c^*\rangle}{2i\omega\langle \mathcal{F}_c|\mathcal{F}_c^*\rangle}\frac{\langle \mathfrak{L}''(\mathbf{u_s})\mathcal{F}_c\mathcal{F}_c|\mathcal{F}_c^*\rangle}{\langle \mathcal{F}_c|\mathcal{F}_c^*\rangle}\right)A|A|^2.$$

Direct calculation for different parameter sets shows, that the correction is much smaller than the coefficient a_2 and thus has no significant contributions. This is also confirmed by numerical results, presented hereafter.

7.2.3 Amplitude equation for three-component RD system

Let us now apply the amplitude equation (7.15) to the three-component system (7.1). To do so one should calculate all scalar products, staying in the coefficients a_1 and a_2. As we mentioned above, the calculation of the eigenfunctions of the adjoint operator $\mathcal{F}^*$, $\overline{\mathcal{F}}_c^*$ is in general rather complicated. But due to decomposition (7.7) the calculation of these functions becomes possible (see the subsection 7.1.3 and the relation (7.10) for details) and one can express all scalar products in (7.16) alone in terms of the critical eigenfunction $\mathcal{F}_c := (\mathcal{F}_{cu}, \mathcal{F}_{cv}, \mathcal{F}_{cw})^T$ of the linearization operator $\mathfrak{L}'(\mathbf{u_s})$.

For example, the scalar product, standing in the numerator of the coefficient a_1 can be presented as

$$\langle \mathfrak{L}'_\varepsilon(\mathbf{u_0})\mathcal{F}_c|\mathcal{F}_c^*\rangle = \langle M_\theta L'(\bar{\mathbf{u}})\mathcal{F}_c|M_c^{-1}\overline{\mathcal{F}}_c\rangle = i\omega\langle M_\theta M_c^{-1}\mathcal{F}_c|M_c^{-1}\overline{\mathcal{F}}_c\rangle = i\omega\kappa_4\langle\mathcal{F}_{cw}^2\rangle,$$

where M_c stands for the matrix M, calculated for the critical value of the control parameter $\theta = \theta_c$, $M_\theta = \frac{\partial M}{\partial\theta}\big|_{\theta=\theta_c}$ and $\langle\mathcal{F}_c^2\rangle = \langle\mathcal{F}_c|\overline{\mathcal{F}}_c\rangle$. The other scalar products in the Eq. (7.16) can be obtained in a similar way. The relations for the coefficients a_1 and a_2 for the system (7.1) take the form:

$$a_1 = \frac{i\omega\kappa_4\langle\mathcal{F}_{cw}^2\rangle}{\langle\mathcal{F}_{cu}^2\rangle - \kappa_3\tau\langle\mathcal{F}_{cv}^2\rangle - \kappa_4\theta_c\langle\mathcal{F}_{cw}^2\rangle},$$
$$a_2 = -\frac{3\langle\mathcal{F}_{cu}^2|\mathcal{F}_{cu}|^2\rangle}{\langle\mathcal{F}_{cu}^2\rangle - \kappa_3\tau\langle\mathcal{F}_{cv}^2\rangle - \kappa_4\theta_c\langle\mathcal{F}_{cw}^2\rangle}$$

and can be immediately evaluated if the solitary stationary solution is known.

7.2.4 Numerical results

In accord with the previous section, all we need to quantify coefficients in Eq. (7.15) is $\mathcal{F}_c$. As this critical eigenfunction is not known analytically we have found it together with the corresponding eigenvalue $i\omega$ and critical value of the control parameter θ_c by solving the eigenvalue problem (7.6) numerically for different values of τ and θ. Based on this, the instability increment $\varepsilon\mathrm{Re}(a_1)$ can be calculated. The latter is presented in Fig. 7.6 as solid triangles, whereas the open squares correspond to the instability increment, derived directly from the system (7.1).

In addition, we have performed direct numerical simulations of the Eq. (7.15) for different values of τ and θ. The results are shown in the Fig. 7.7. Figure 7.7 (a) demonstrates a typical solution of the Eq. (7.15) in the case of nonlinear stabilization, i.e., for $\mathrm{Re}(a_1) > 0$ and $\mathrm{Re}(a_2) < 0$. In this

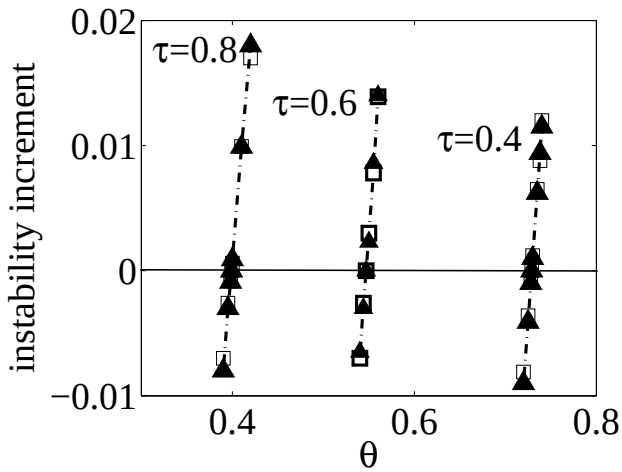

FIG. 7.6: Dependence of the instability increment $\varepsilon\mathrm{Re}(a_1)$ on the control parameter θ for three different τ as results from the reduced model (7.15) (▲) and direct simulation of the system (7.1) (□). Other parameters are: $D_u = 4.7 \cdot 10^{-3}$, $D_v = 0$, $D_w = 0.01$, $\lambda = 5.67$, $\kappa_1 = -1.04$, $\kappa_3 = 1.0$, $\kappa_4 = 3.33$.

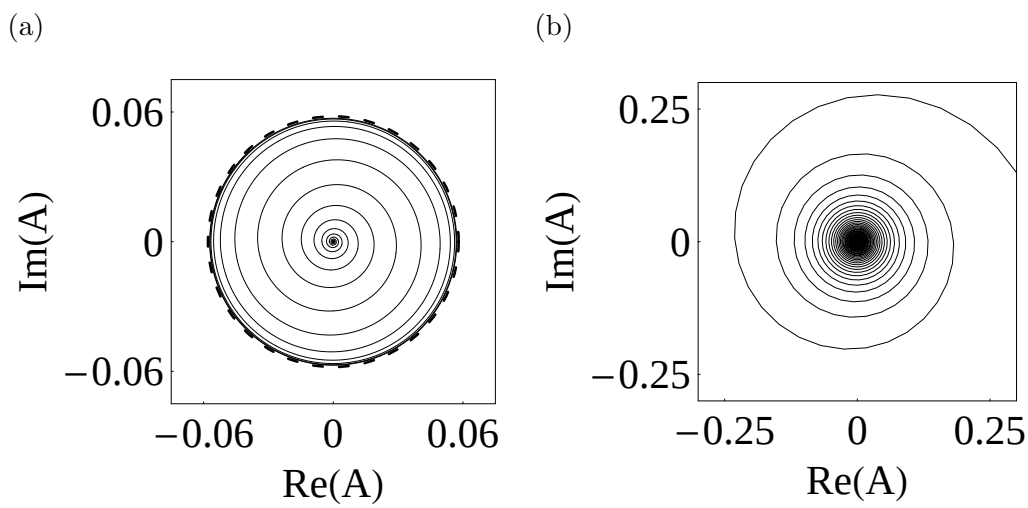

FIG. 7.7: Numerical solutions of the Eq. (7.15) on the phase plane (Re(A), Im(A)) in super- and subcritical regimes. (a) The typical solution of the amplitude equation for $\mathrm{Re}(a_2) > 0$, calculated for $\tau = 0.5$, $\theta = 0.65$. The dotted line corresponds to the limit circle, obtained as the solution of the full three-component system. (b) The typical solution of the reduced system for $\mathrm{Re}(a_2) < 0$. Control parameters are $\tau = 0.7$ and $\theta = 0.55$. Other parameters are the same as in the Fig. 7.6.

case the solution on the complex plane is represented by a unstable focus surrounded by a stable limit cycle of the radius $R = \sqrt{-\varepsilon \frac{\mathrm{Re}(a_1)}{\mathrm{Re}(a_2)}}$. It is necessary to stress that a direct calculation of the complex amplitude $A(t)$ for all t from the system (7.1) involves some difficulties, while the derivation of the limit cycle radius is relatively simple. The latter can be seen in the Fig. 7.7 (a) as a dotted line.

In Figure 7.7 (b) a typical solution, corresponding to the subcritical regime with $\mathrm{Re}(a_1) > 0$, $\mathrm{Re}(a_2) > 0$, is shown. In this case the solution on the phase plane corresponds to the unstable focus. In order to compare this result with the full model, direct simulations of the system (7.1) for the same parameter set have been performed; the obtained solution clearly shows absence of the nonlinear stabilization, i.e, the stationary solution becomes unstable and starts to oscillate with an increasing amplitude that finally leads to destruction of the solution by the oscillations.

It should be mentioned that similar to [Haim et al., 1996], further increase of the control parameter in the supercritical regime can also lead to the destruction of the limit cycle and collapse of the soliton. The latter transition cannot be described by Eq. (7.15). Indeed, the amplitude equation (7.15) is derived in the vicinity of the bifurcation point θ_c, i.e., the sign of the coefficients a_1 and a_2 is calculated in this critical point. Predictions far from the bifurcation point are therefore impossible. On the other hand, numerical simulations show that the destruction of the limit cycle usually takes place far beyond the vicinity of the bifurcation point and are out of scope of the amplitude equation (7.15).

7.3 Destabilization via the mode $n = 1$: Drift-Bifurcation

7.3.1 Drift-Bifurcation due to a change of time constant

In this section we consider the influence of the mode with $n = 1$ on the dynamic of DS. As noted above the system (7.1) is neutral stable, i.e., $\lambda = 0$ is the eigenvalue of the operator $\mathfrak{L}'(\mathbf{u_s})$, corresponding to two independent neutral eigenfunctions (one for each spatial direction) $\mathcal{G}_\mathbf{r}$, $\mathbf{r} = x, y$. However, a slight disturbance of $\mathbf{u_s}$ in the form of $\mathcal{G}_\mathbf{r}$, causes only a translation of the stationary solution, its stability is not affected. The typical destabilization scenario is that the real part of eigenvalue $\mathrm{Re}(\lambda)$ passes through zero as one gradually changes the parameters of the system (see e.g, section 7.2 for details). In the following we consider the case that $\mathrm{Im}(\lambda)$ also passes through zero [Or-Guil et al., 1998]. Figure 7.8 shows such eigenvalues dynamics on the complex plane $(\mathrm{Re}(\lambda), \mathrm{Im}(\lambda))$ by the change of the control parameter τ, while θ is kept fixed. One can see, that at the beginning all eigenvalues are situated on the real axis. By the change of τ all λ but $\lambda = 0$ start to move. As well as

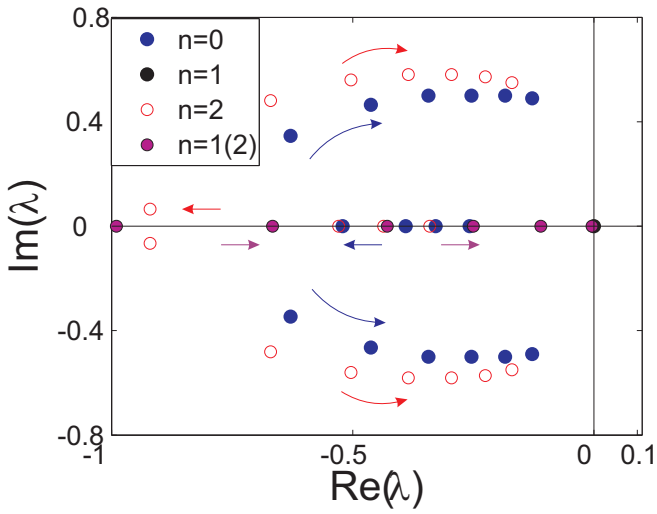

FIG. 7.8: Typical eigenvalues behavior on the complex plane (Re(λ), Im(λ)) by the change of τ in case that the mode $n = 1$ becomes excited first. The eigenvalues corresponding to different eigenfunctions differs in colors (see the legend). The accordingly colored arrows show the motion direction of the eigenvalues on the complex plane by the change of the control parameter.

in section 7.2 (see Fig. 7.4), all eigenvalues, corresponding to eigenmodes with small n move first in opposite to Im(λ) direction and become complex afterwards (see Fig. 7.8 for modes $n = 0$ and $n = 2$). But in the case presented here, one mode (purple colored one), denoted in Fig. 7.8 as $n = 1(2)$ remains on the real axis and moves in the Im(λ) direction. Finally, this eigenvalue achieves the zero far in advance of other modes. The corresponding eigenfunction can be represented as a linear combination of the Goldstone modes. The system of eigenfunctions is then incomplete and has to be supplemented with a generalized eigenfunction with eigenvalue zero, the so-called *propagator mode* $\mathcal{P}_{\mathbf{r}}$ [Or-Guil et al., 1998, Schütz, 1995], which is defined by the relation

$$\mathfrak{L}'(\mathbf{u_s})\mathcal{P}_{\mathbf{r}} = \mathcal{G}_{\mathbf{r}}. \tag{7.17}$$

The occurrence of the propagator mode marks the onset of the destabilization, therefore the value of the control parameter for which Eq. (7.17) is fulfilled corresponds to the bifurcation point. The stationary solution becomes unstable at this point due to the existence of this generalized mode: a perturbation in form of the propagator mode causes a change in form of the Goldstone mode that corresponds to a permanent shift of the DS [Or-Guil et al., 1998]. Thus we have a transition from a stationary to a moving state, i.e., *a drift bifurcation*.

Using the Fredholm alternative, it can be proven that Eq. (7.17) can be

solved if and only if the equality

$$\langle \mathcal{G}^*_{\mathbf{r}} | \mathcal{G}_{\mathbf{r}} \rangle = 0 \tag{7.18}$$

is fulfilled, where $\mathcal{G}^*_{\mathbf{r}}$ is an eigenfunction of the adjoint operator $\mathfrak{L}'^{\dagger}(\mathbf{u_s})$ with the eigenvalue zero and the same spatial symmetry as $\mathcal{G}_{\mathbf{r}}$.

Remark: As is shown in subsection 7.1.3, in general the condition (7.18) is not fulfilled and becomes correct only in degeneration point, where instability takes place (bifurcation point).

As we mentioned above, the analytic calculation of the eigenfunctions $\mathcal{G}^*_{\mathbf{r}}$ of the adjoint operator $\mathfrak{L}'^{\dagger}(\mathbf{u_s})$ poses severe problems, but in the present case it is possible due to the special form (7.7) of the operator $\mathfrak{L}'(\mathbf{u_s})$. For a given Goldstone mode $\mathcal{G}_{\mathbf{r}}$, the eigenfunction $\mathcal{G}^*_{\mathbf{r}}$ can be calculated via the relation (7.11),

$$\mathcal{G}^*_r = M^{-1}\mathcal{G} = \begin{pmatrix} \frac{\partial \mathbf{u_s}}{\partial \mathbf{r}} \\ -\kappa_3 \tau \frac{\partial \mathbf{v_s}}{\partial \mathbf{r}} \\ -\kappa_4 \theta \frac{\partial \mathbf{w_s}}{\partial \mathbf{r}} \end{pmatrix}.$$

In the following, we will without loss of generality restrict ourselves to the case $\mathbf{r} = x$ as all spatial directions are equal. In this case the perturbed solution will move in the x-direction. Let us define $\tau_{c,x}$ as the value of the parameter τ for which condition (7.18) is fulfilled. Consequently, condition (7.17) will be fulfilled for the same τ as well. The value $\tau_{c,x}$ can be calculated by inserting the explicit expressions for $\mathcal{G}_x$ and $\mathcal{G}^*_x$ into Eq. (7.18), which results in the algebraic equation

$$\langle u^2_{s,x} \rangle - \kappa_3 \tau_{c,x} \langle v^2_{s,x} \rangle - \kappa_4 \theta \langle w^2_{s,x} \rangle = 0, \tag{7.19}$$

yielding the expression

$$\tau_{c,x} = \frac{\langle u^2_{s,x} \rangle - \kappa_4 \theta \langle w^2_{s,x} \rangle}{\kappa_3 \langle v^2_{s,x} \rangle}, \tag{7.20}$$

where $\mathbf{u}_{s,x} := \frac{\partial \mathbf{u_s}}{\partial x}$. For $\theta = 0$ and $D_v = 0$ this expression has been derived in [Or-Guil et al., 1998]. Here we consider a more complicated three-component system with $D_v = 0$ but $\theta > 0$. In this situation, Eq. (7.20) can be rewritten in the form

$$\tau_{c,x} = \frac{1}{\kappa_3} - \theta \frac{\kappa_4}{\kappa_3} \frac{\langle w^2_{s,x} \rangle}{\langle u^2_{s,x} \rangle}. \tag{7.21}$$

Our next goal is to examine the dependence of the velocity c of a DS on the system parameters in the vicinity of the bifurcation point $\tau = \tau_{c,x}$. For this purpose we transform the system (7.1) into a coordinate frame moving with the velocity c in the x-direction by means of the substitution $x \rightarrowtail x - ct$. The transformed equations read

$$\begin{aligned} u_t &= c u_x + D_u \Delta u + \lambda u - u^3 - \kappa_3 v - \kappa_4 w + \kappa_1, \\ v_t &= c v_x + (u - v)/\tau, \\ w_t &= c w_x + (D_w \Delta w + u - w)/\theta. \end{aligned} \tag{7.22}$$

A stationary solution $\widehat{\mathbf{u}}_s = (\hat{u}, \hat{v}, \hat{w})^T$ of Eq. (7.22) corresponds to a uniformly moving DS. Note that the rotational symmetry can not be expected any more. After projecting the system (7.22) for $\mathbf{u} = \widehat{\mathbf{u}}_s$ onto the vector function $(\hat{u}_x, -\kappa_3\tau\hat{v}_x, -\kappa_4\tau\hat{w}_x)$ and performing several transformations, most of which consist of taking integrals by parts, one obtains the expression

$$c(\langle\hat{u}_x^2\rangle - \kappa_3\tau\langle\hat{v}_x^2\rangle - \kappa_4\theta\langle\hat{w}_x^2\rangle) = 0. \tag{7.23}$$

In order to rewrite Eq. (7.23) into a more suitable form we take use of the second equation of Eqs. (7.22), rewriting it for the case of a stationary solution $\widehat{\mathbf{u}}_s$, i.e.

$$\hat{u} = \hat{v} - c\tau\hat{v}, \tag{7.24}$$

and insert the latter in (7.23) to obtain the following result:

$$c\tau^2\langle\hat{v}_{xx}^2\rangle\left[c^2 - \frac{\kappa_3}{\tau^2}\frac{\langle\hat{v}_x^2\rangle}{\langle\hat{v}_{xx}^2\rangle}\left(\tau - \left(\frac{1}{\kappa_3} - \theta\frac{\kappa_4}{\kappa_3}\frac{\langle\hat{w}_x^2\rangle}{\langle\hat{v}_x^2\rangle}\right)\right)\right] = 0, \tag{7.25}$$

In the vicinity of the bifurcation point $\tau \approx \tau_{c,x}$, $\hat{u} \approx \hat{v} \approx u_s$ and $\hat{w} \approx w_s$. Thus we can rewrite expression (7.25) as

$$c\tau_{c,x}^2\langle u_{s,xx}^2\rangle\left[c^2 - \frac{\kappa_3}{\tau_{c,x}^2}\frac{\langle u_{s,x}^2\rangle}{\langle u_{s,xx}^2\rangle}\left(\tau - \tau_{c,x}\right)\right] = 0. \tag{7.26}$$

For $\tau \leq \tau_{c,x}$, only the trivial solution $c = 0$ of Eq. (7.26) exists and no travelling DSs are observed. The situation is different for $\tau > \tau_{c,x}$ as one obtains two additional finite solutions of the last equation:

$$c^2 = \frac{\kappa_3}{\tau_{c,x}^2}\frac{\langle u_{s,x}^2\rangle}{\langle u_{s,xx}^2\rangle}\left(\tau - \tau_{c,x}\right). \tag{7.27}$$

The additional solutions indicate a drift bifurcation at $\tau_{c,x}$ due to a change of the time scale constant τ. On the other hand, for a fixed τ the drift bifurcation can also be induced by shifting the bifurcation point $\tau_{c,x}$ (7.21) due to a variation of the stationary solution $(u_s, v_s, w_s)^{\mathrm{T}}$. To do this, every parameter which does not destroy the integrity of the DS is appropriate.

In particular, parameter κ_1 is an appropriate candidate. Indeed, as is mentioned in the Chapter 5, κ_1 is related to the normalized applied voltage in the experimental system. From the experimental point of view, the change of the applied voltage also leads to the destabilization of the current filament in form of drift-bifurcation [Gurevich et al., 2004b]. Thus, using κ_1 as the control parameter one can qualitatively compare the results of experimental and theoretical findings. This is the aim of the next two sections.

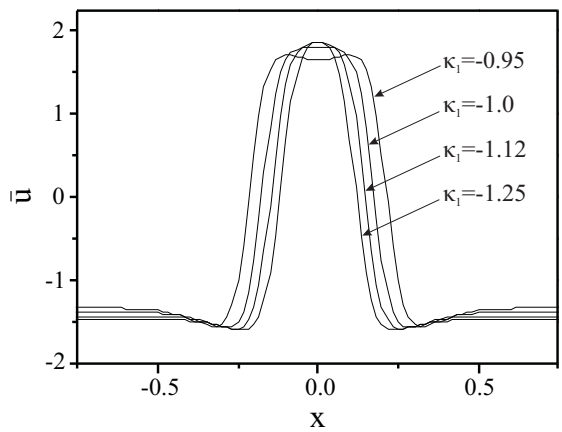

FIG. 7.9: Shape of the stationary activator distribution $\mathbf{u}_s$ for different values of κ_1. Parameters: $D_u = 4.67 \times 10^{-3}$, $D_v = 0$, $D_w = 0.01$, $\lambda = 5.67$, $\theta = 0.1$, $\tau = 1.2$, $\kappa_3 = 1$, $\kappa_4 = 3.33$.

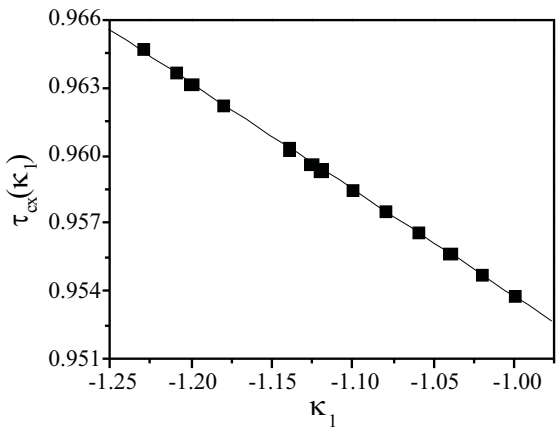

FIG. 7.10: Dependence of the critical value $\tau_{c,x}$ on the control parameter κ_1. Parameters: $D_u = 4.67 \times 10^{-3}$, $D_v = 0$, $D_w = 0.01$, $\lambda = 5.67$, $\theta = 0.1$, $\tau = 1.2$, $\kappa_3 = 1$, $\kappa_4 = 3.33$, $\kappa_1 \in [-1.25, -0.95]$.

7.3.2 Drift-Bifurcation due to a change of shape

Analyzing the solutions of (7.1) using κ_1 as control parameter, one finds that the shape of the stationary solution $(u_s, v_s, w_s)^T$ is directly affected by changes of κ_1 (see Fig. 7.9). Therefore, we consider $\mathbf{u}_s$ as a function of κ_1 and rewrite Eq. (7.21) as

$$\tau_{c,x} = \frac{1}{\kappa_3} - \theta \frac{\kappa_4}{\kappa_3} \frac{\langle u_{s,x}^2(\kappa_1) \rangle}{\langle u_{s,x}^2(\kappa_1) \rangle} = \tau_{c,x}(\kappa_1). \tag{7.28}$$

According to Eq. (7.28), there is a dependence between the control parameter κ_1 and the critical value of the parameter τ (see Fig. 7.10). If the stationary distribution of $\mathbf{u}_s(\kappa_1)$ is known, the velocity c can be determined as a function

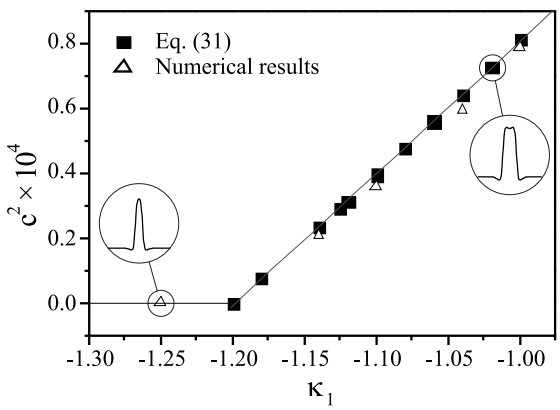

FIG. 7.11: Dependence of the square of the DSs velocity c^2 on the control parameter κ_1 as results of analytical (■) and numerical calculations (△). Parameters: $D_u = 4.67 \times 10^{-3}$, $D_v = 0$, $D_w = 0.01$, $\lambda = 5.67$, $\theta = 0.1$, $\tau = 1.2$, $\kappa_3 = 1$, $\kappa_4 = 3.33$, $\kappa_1 \in [-1.25, -0.95]$.

of κ_1, i.e.

$$c^2 = \frac{\kappa_3}{\tau_{c,x}^2(\kappa_1)} \frac{\langle u_{s,x}^2(\kappa_1)\rangle}{\langle u_{s,xx}^2(\kappa_1)\rangle} \Big(\tau - \tau_{c,x}(\kappa_1)\Big) =: f(\kappa_1). \tag{7.29}$$

In order to investigate the dependence of c^2 on the control parameter κ_1 one has to find stationary solutions of Eq. (7.1) in form of DSs. As these solutions are not known analytically we have solved (7.1) numerically for different values of the parameter κ_1 while keeping all other parameters fixed. Based on these stationary solutions, Eqs. (7.28) and (7.29) have been evaluated. The results are presented in Fig. 7.11 as solid squares, whereas the solid inclined line is a linear fit of this data. Additionally, we have performed numerical simulations of the system (7.1) starting from the disturbed stationary DSs and determined the equilibrium velocities of the DSs for various values of κ_1. The results are presented in Fig. 7.11 as open triangles. It can be seen that both methods up to a small numerical error provide the same functional dependency of the velocity c on the control parameter κ_1. The results demonstrate that DSs can undergo a drift bifurcation from a stationary to a travelling state which is induced by a shift of the bifurcation point due to a continuous change of shape of the DS. The experimental findings, showing the drift-bifurcation of current filaments due to change of shape in dc gas-discharge system are presented below.

7.3.3 Experimental observations

The investigated dc gas-discharge system and ,in particular, experimental set-up are discussed in Sec. 2.3.1 of Chapter 2. As is shown there, when some control parameter, say, the supply voltage U_0 is increased beyond the ignition voltage, various forms of spatially inhomogeneous self-organized luminance pat-

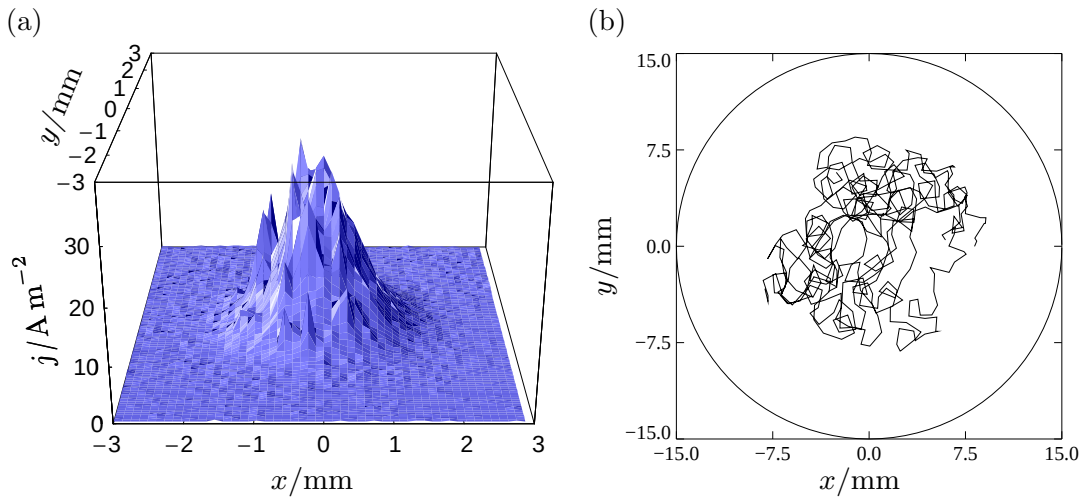

FIG. 7.12: (a) Experimentally recorded current density distribution of a propagating filament in one frame. (b) Trajectory of the center of the distribution in the discharge plane, the circle indicates the mechanical boundary of the discharge area. Parameters: external voltage $U_0 = 2800\,\mathrm{V}$, resistivity of the semiconductor $\rho_{SC} = 1.83 \cdot 10^6\,\Omega \cdot \mathrm{cm}$, series resistor $R_0 = 10\,\mathrm{M}\Omega$, pressure $p = 280\,\mathrm{hPa}$, temperature $T = 100\,\mathrm{K}$, with of the discharge gap $d = 500\,\mu\mathrm{m}$, exposure time $t_{exp} = 0.02\,\mathrm{s}$.

terns can be observed in the discharge gap [Astrov and Logvin, 1997, Astrov et al., 1997, Ammelt et al., 1998, Strümpel et al., 2001, Gurevich et al., 2003a]. Here we concentrate on current filaments, for which characteristic interaction processes like scattering, the formation and decay of bound states as well as generation and annihilation are observed [Astrov and Purwins, 2001, Astrov and Logvin, 1997, Bödeker et al., 2004]. Due to the solitary properties of the filaments and the dissipativity of the gas-discharge system, we will in the following consider the filaments as dissipative solitons. As the CCD camera records the luminance distribution in a plane perpendicular to the discharge direction, the originally planar, but three-dimensional filaments are observed as two-dimensional bright spots. It can be shown that the observed luminance intensity is locally proportional to the average current density in the discharge direction.

Here the parameters of the discharge system are chosen in such a way that only one filament is exited. In this way, any possible interaction of filaments is excluded. While doing the experiment, great care is taken to ensure a high spatial homogeneity of the system (for details see [Bödeker et al., 2003]) since inhomogeneities may influence the dynamics of the filaments and possibly lead to non-self-organized patterns. Fig. 7.12.a shows the current density profile of a single propagating filament recorded under the named conditions. The basic shape of the structure remains conserved during the propagation, although slight deviations from an ideal radially symmetric shape can be ob-

served. Therefore it seems sensible to describe the propagation of the whole filament in terms of the two-dimensional trajectory of the "center of mass" of its current density distribution, corresponding to a particle approach. To this end, the filament in each recorded frame is identified as a region of high luminance density and the corresponding center of luminance (which corresponds to the center of the current density distribution) is calculated [Bödeker et al., 2003]. The resulting trajectory for the shown example is depicted in Fig. 7.12.b. Obviously, a possible deterministic part of the motion of the filament is superimposed by stochastic contributions.

As discussed in [Bödeker et al., 2003], the deterministic motion of the filaments cannot be determined directly from the trajectories. To overcome this drawback, we apply an appropriate stochastic data analysis technique [Bödeker et al., 2003, Siegert et al., 1998], which is briefly discussed below.

We start with a general introduction to methods of stochastic data analysis and their applications. Afterwards we apply the techniques to the dynamics of experimentally observed DSs in the semiconductor gas-discharge system.

In order to describe the dynamics of a continuous Markovian system and a wide variety of stochastic dynamical systems one often uses a Langevin equation [Kittel, 1958]

$$\frac{d}{dt}q_i(t) = h_i(\{q_k(t)\}, t) + g_{ij}(\{q_k(t)\}, t)\Gamma_j(t), \;\; i, j = 1 \ldots n \tag{7.30}$$

for a set of n random variables $\boldsymbol{q} = \{q_k(t)\}$, $k = 1 \ldots n$. Here the first term on the right side describes the deterministic part of the dynamics of the system whereas the second term relates to the stochastic part, representing the influence of noise. The latter is a product of the matrix of amplitudes of noise $\boldsymbol{g}(\boldsymbol{q}, t) = \{g_{ij}(\boldsymbol{q}, t)\}$ and a vector $\boldsymbol{\Gamma}$ of n fluctuating Langevin forces, which are usually assumed to be δ-correlated noise forces with vanishing mean:

$$\langle \Gamma_i(t) \rangle = 0 \qquad i = 1 \ldots n, \tag{7.31}$$

$$\langle \Gamma_i(t)\Gamma_j(t') \rangle = 2\delta_{ij}\delta(t - t') \qquad i, j = 1 \ldots n. \tag{7.32}$$

Here δ_{ij} is the Kronecker symbol, $\delta(t - t')$ is the delta function and $\langle \cdot \rangle$ denotes the ensemble average. According to Wiener-Khintchine's theorem [Kittel, 1958], Eq. (7.32) characterizes the fluctuations as white noise.

Following [Risken, 1996], a Fokker-Planck equation can be found for each Langevin equation fulfilling (7.31) and (7.32). This allows us to write down the following relations for the deterministic and the stochastic terms (see [Risken, 1996]):

$$h_i(\boldsymbol{q}) = \lim_{\triangle t \to 0} \frac{1}{\triangle t} \langle q_i'(t + \triangle t) - q_i'(t) \rangle \mid_{\boldsymbol{q}'(t) = \boldsymbol{q}}, \tag{7.33}$$

$$g_{ik}(\boldsymbol{q})g_{jk}(\boldsymbol{q}) = \frac{1}{2} \lim_{\triangle t \to 0} \frac{1}{\triangle t} \langle (q_i'(t + \triangle t) - q_i'(t))(q_j'(t + \triangle t) - q_j'(t)) \rangle \mid_{\boldsymbol{q}'(t) = \boldsymbol{q}} \tag{7.34}$$

where $\boldsymbol{q}'(t)$ is assumed to be a solution of Eq. (7.30). For Eq. (7.33), the fluctuation term in (7.30) is interpreted according to the Itó calculus. Note that in real physical systems, condition (7.31) can always be fulfilled whereas Eq. (7.32) approximately holds as long as the noise correlation time is smaller than the characteristic time scale of the investigated dynamics. Moreover, in real systems only a finite number of data points is available. In order to use conditions (7.33) and (7.34) in practice, one has to use a finite time interval $\triangle t$, ensuring that $\triangle t$ is smaller than the characteristic time scale of the dynamics of the system, but larger than the correlation time of the fluctuations [Siegert et al., 1998, Friedrich et al., 2000]. This yields

$$h_i(\boldsymbol{q}) + g_{kj}(\boldsymbol{q})\frac{\partial}{\partial q_k}g_{ij}(\boldsymbol{q}) \approx \frac{1}{\triangle t}\langle q_i'(t+\triangle t) - q_i'(t)\rangle \mid_{\boldsymbol{q}'(t)\approx\boldsymbol{q}}, \tag{7.35}$$

$$g_{ik}(\boldsymbol{q})g_{jk}(\boldsymbol{q}) \approx \frac{1}{2}\frac{1}{\triangle t}\langle (q_i'(t+\triangle t) - q_i'(t))(q_j'(t+\triangle t) - q_j'(t))\rangle \mid_{\boldsymbol{q}'(t)\approx\boldsymbol{q}} . \tag{7.36}$$

In order to apply this approach to the dynamics of the DSs in the experimental gas-discharge system, we use a particle ansatz in which the dynamics of each filament is described using its center of luminance $\boldsymbol{r}(t) = (r_x(t), r_y(t))^T$ and its velocity $\dot{\boldsymbol{r}}(t) = \boldsymbol{v}(t) = (v_x(t), v_y(t))^T$ as dynamic variables. Using the translational and rotational invariance of the system which for our experimental set-up can be achieved by a homogeneous preparation of the discharge area (under negligence of the finite size of the system) and taking into account the strong dissipation of the gas-discharge system, the following Langevin equation describing the dynamics of a single filament without interaction has been derived [Bödeker et al., 2003, Liehr et al., 2003]:

$$\dot{\boldsymbol{v}} = \boldsymbol{h}(\boldsymbol{v}) + \boldsymbol{R}(\boldsymbol{v})\boldsymbol{\Gamma}(t). \tag{7.37}$$

Here $\boldsymbol{h}$ describes the deterministic motion of the soliton, whereas the second term represents the influence of noise. It consists of a matrix of noise amplitudes $\boldsymbol{R}(\boldsymbol{v})$ and a fluctuation force $\boldsymbol{\Gamma}$. As we mentioned above, in order to apply Eqs. (7.33) and (7.34) we assume Eq. (7.32) to be fulfilled on the timescale of the motion of filaments, Eq. (7.31) can always be fulfilled by introducing an offset in $\boldsymbol{h}$. Under these conditions, using Eq. (7.36) one can obtain the deterministic part of the dynamics through Eq. (7.33), showing that $\boldsymbol{h}$ possesses radial symmetry with respect to $\boldsymbol{v}$ (for details see [Bödeker et al., 2003]). Thus one can rewrite Eq. (7.37) in the form

$$\dot{\boldsymbol{v}} = h_v(v)\boldsymbol{e_v} + R(v)\,\boldsymbol{\Gamma}(t). \tag{7.38}$$

Here $v = |\boldsymbol{v}|$, $\boldsymbol{e_v} = \boldsymbol{v}/v$ and $h_v(v)$ is a projection of the vector $\boldsymbol{h}$ on the unit vector of the velocity $\boldsymbol{v}$, i.e. $\boldsymbol{h}(\boldsymbol{v}) = h_v(v)\boldsymbol{e_v}$.

Transforming Eq. (7.38) into polar coordinates, one can prove that the deterministic part of the dynamics can be calculated via (cf. [Bödeker et al.,

2003])

$$h_v(v)\frac{R^2(v)}{v} + R(v)\frac{\partial R(v)}{\partial v} \approx \frac{1}{\Delta t}\left\langle |\boldsymbol{v}'(t+\Delta t)| - |\boldsymbol{v}'(t)| \right\rangle\Big|_{|\boldsymbol{v}'(t)|\approx v} \tag{7.39}$$

where $\boldsymbol{v}'(t)$ is solution of Eq. (7.38). In the practical analysis of the experimental data using Eq. (7.39) is inconvenient as the fluctuation term on the left-hand side of the equation has to be determined each time. This drawback can be overcome by using the following "projection", allowing for an estimation of the function $h_v(v)$ without determining $R(v)$ [Bödeker et al., 2003, Liehr et al., 2003]:

$$h_v(v) \approx \frac{1}{\Delta t}\left\langle \frac{(\boldsymbol{v}'(t+\Delta t) - \boldsymbol{v}'(t)) \cdot \boldsymbol{v}'(t)}{|\boldsymbol{v}'(t)|} \right\rangle\Bigg|_{|\boldsymbol{v}'(t)|\approx v}. \tag{7.40}$$

Due to the utilization of the radial symmetry and the estimation in a single step, Eq. (7.40) provides a powerful tool to determine the deterministic dynamics of a single filament despite the presence of strong fluctuations.

So, using methods of stochastic data analysis, it is possible to determine the deterministic dynamics of a single filament by estimating the function $h_v(v)$. Recent investigation have shown that $h_v(v)$ always has one stable fixed point v_0 (given by $h(v_0) = 0$ and $h'(v_0) < 0$), corresponding to the "'intrinsic velocity"' of the filament. Furthermore, it was found that a single filament can undergo a bifurcation, i.e. a transition from a vanishing to a finite intrinsic velocity, by using the specific resistivity ρ_{sc} of the semiconductor cathode as control parameter [Bödeker et al., 2003]. In the experiment, the value ρ_{sc} can be varied via external illumination, which requires a calibration of the nonlinear dependence of the specific resistivity on the light intensity, rendering the specific resistivity as a suitable but uncomfortable control parameter.

As a consequence, the question arises if it is possible to find a drift bifurcation of localized structures in the experimental system using other control parameters. A straight forward decision is the global voltage U_0 applied to the discharge cell, since U_0 is easy to change and to control. This control parameter has also been applied in the context of other bifurcation scenarios, e.g., the Turing destabilization of a homogeneous discharge [Ammelt et al., 1997] or the self-completion of single filaments [Astrov and Logvin, 1997], which leads to the generation of additional filaments. However, for the parameters chosen in the current investigation, a single filament is stable for a large range of parameters and initial conditions.

An application of the stochastic data analysis to experimentally recorded data series shows that changing U_0 does not only cause a significant change of the shape of the averaged filament shape (see Fig. 7.13), but also leads to a change of the dynamics of the filament, which becomes clear when plotting the square of the intrinsic velocity v_0 as a function of the control parameter U_0

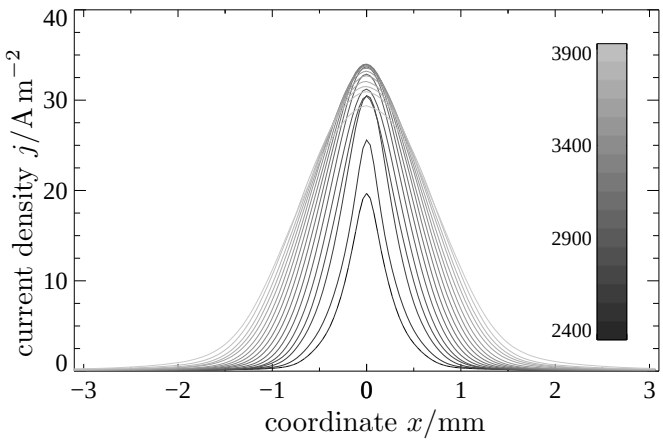

FIG. 7.13: Central transverse section of the luminance distribution of the filament for different values of U_0, parameters like in Fig. 7.12. For each section, 4000 frames were shifted to the center of the distribution and averaged to exclude different fluctuations. Note that with increasing voltage, the maximum luminance intensity grows and starts to decrease again at a voltage $U_{\mathrm{th}} \approx 2800\,\mathrm{V}$.

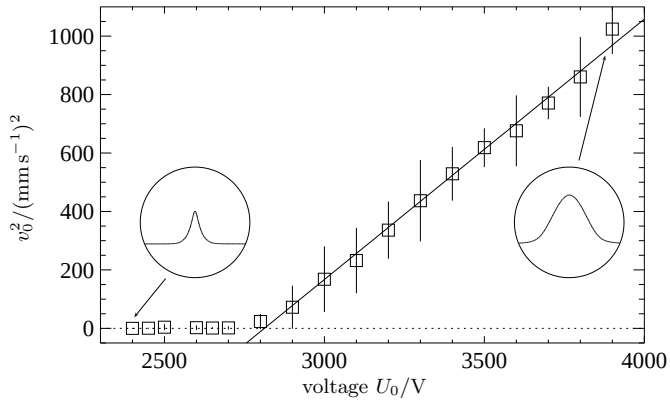

FIG. 7.14: Experimentally measured drift bifurcation using the voltage U_0 as control parameter. Parameters like in Fig. 7.12.

(Fig. 7.14). The plot shows that below a critical value $U_0 = U_{crit} \approx 2800\,\mathrm{V}$ of the control parameter, the intrinsic velocity of the filament vanishes, so that its motion observed in the experiment is purely noise-induced like for a Brownian particle, whereas for $U_0 > U_{crit}$ the filament starts to move intrinsically with a finite velocity v_0. In this case the filament would also propagate in the absence of noise. This transition can be interpreted as *drift bifurcation* from a stationary to a moving state, which in the present case is hidden by noise. It is noticeable that above the bifurcation point, the square of the intrinsic velocity scales linearly with the control parameter, showing a bifurcation similar to the theoretical finding (Fig. 7.11). This observation rises the question if the bifurcation and the characteristic scaling behavior of the intrinsic velocity can be related to the change of the shape of the filament, which is caused by increasing the supply voltage.

Note that the qualitative agreement of the experimental system and the theoretical model show that the drift-bifurcation of DSs can occur in rather general scenarios in which the destabilization is accompanied or induced by a significant but continuous change of the shape of the DSs, induced by varying an appropriate control parameter.

7.4 Travelling and breathing DSs: codim=2 point

As was shown in sections 7.2 and 7.3, in order to become the mode $n = 0$ or $n = 1$ excited only one control parameter has to be changed. Here, we are interested in more complicated situation, where both modes becomes unstable simultaneously (see Fig. 7.15). In this case two control parameters are to be changed, so one can speak about codim=2 bifurcation point. We start from the numerical analysis of such kind of bifurcation for single DS, restricting ourself on the case of monotonic tails.

7.4.1 One-soliton solution

We have performed two series of numerical simulations of the system (7.1) in the vicinity of the codim=2 bifurcation point (τ_c, θ_c). The first one was made for fixed τ_c and three different values of θ. The results of simulations are depicted in Fig. 7.16. If θ is chosen to be close to θ_c, an initial pulse close to the stationary solution converges to moving and breathing with a constant amplitude DS, as shown in Fig. 7.16 (a). Notice that dependence of the DS position on time is not linear, as in the case of drift bifurcation, but is proportional to $\sqrt{t}$ (see Fig. 7.16 (d)). Here the black line represents the numerically calculated dependence of the soliton's position on time, whereas the red curve is a fit of this data with a function $c_1\sqrt{t} + c_2$. This implies, that single DS in this case moves with nonconstant velocity, proportional to $1/\sqrt{t}$, as shown in Fig. 7.17.

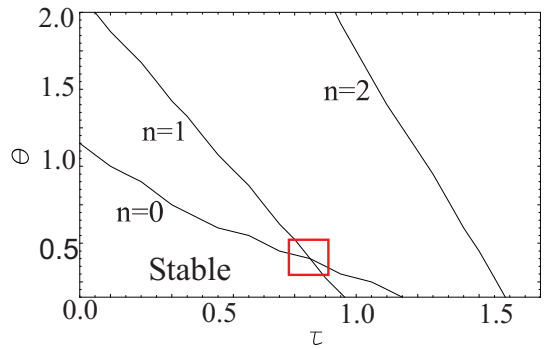

FIG. 7.15: Stability diagram in (τ, θ) plane, calculated for a solitary solution of the system (7.1). Lines separate stability regions, corresponding to different modes n=0,1,2. Parameters: $D_u = 4.7 \cdot 10^{-3}$, $D_v = 0$, $D_w = 0.01$, $\lambda = 5.67$, $\kappa_1 = -1.04$, $\kappa_3 = 1.0$, $\kappa_4 = 3.33$. The rot square denotes the vicinity of the codim=2 bifurcation point we are interested in.

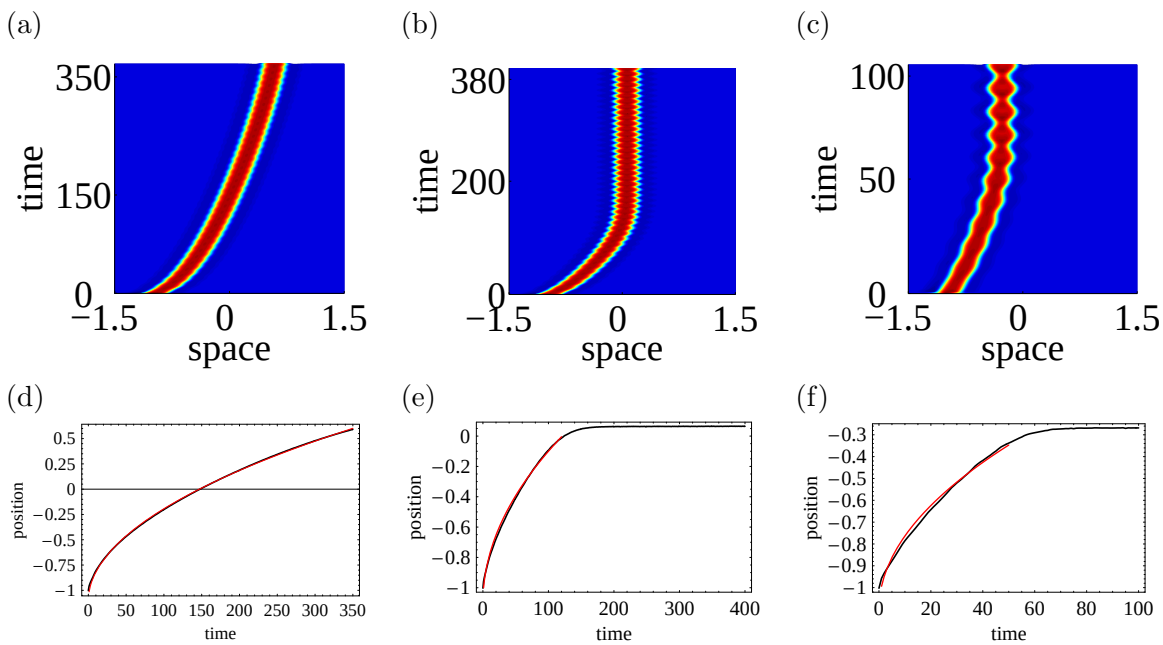

FIG. 7.16: Space-time plots of the activator u for different values of θ obtained from numerical solution of (7.1). Time evolution of the cross-section of the initial pulse close to the stationary solution as well as the time dependence of the soliton's position are shown; a) $\theta = 0.38$ b) $\theta = 0.4$ c) $\theta = 0.44$. Other parameters: $D_u = 4.7 \cdot 10^{-3}$, $D_v = 0$, $D_w = 0.01$, $\lambda = 5.67$, $\kappa_1 = -1.04$, $\kappa_3 = 1.0$, $\kappa_4 = 3.33$, $\tau = 0.834$. The codim=2 bifurcation point is $(\tau_c, \theta_c) = (0.834, 0.376)$. The calculations was performed on the rectangular domain $\Omega = [-1.5, 1.5] \times [-1.5, 1.5]$ on nonuniform triangular grid with maximal element size 0.12 with Neumann boundary conditions.

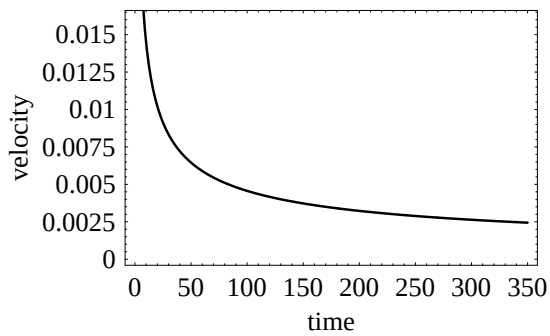

FIG. 7.17: Time dependence of velocity of the single moving and breathing DS in the vicinity of the codim=2 bifurcation point. Parameters are the same as in Figs. 7.16 (a,d).

However the behavior of the DS changes if one increases θ further (see Fig. 7.16 (b)). In this case at the beginning the position of DS is also proportional to $\sqrt{t}$, whereas the oscillation amplitude increases. After some time the soliton stops (see Fig. 7.16 (e)), and oscillation amplitude reaches some constant value. So finally one obtains a stationary breathing with constant amplitude DS. Further increase of the θ makes no significant changes in the dynamics of DS. At the beginning of the simulation initial pulse starts to move with the velocity $\sim 1/\sqrt{t}$ and oscillate with increasing amplitude, but in the short run the soliton's velocity becomes zero and breathing amplitude reaches the constant value (see Figs. 7.16 (c,f)).

The second simulation series is performed for τ and θ values, which are slightly different from (τ_c, θ_c). As before, one fixes one of the control parameter (e.g., τ) and changes the second one. The results are shown in Fig. 7.18. In Figure 7.18 (a) moving and breathing DS is shown. In contrast to the first simulation series, the soliton here moves with a constant velocity. The oscillation amplitude decreases, so finally one has just moving with a constant velocity DS. Another example is shown in Figure 7.18 (b). Here initial pulse converges to the moving with the constant velocity and breathing with a constant amplitude DS. Further increase of the control parameter destroys the solution (see Fig.7.18 (c)).

Both simulation series indicate the difference in dynamics of single DS in the vicinity of the codim=2 bifurcation point. The latter may be explained with the fact that the corresponding critical eigenmodes $n = 0$ and $n = 1$ have different increments, and consequently different influences on the dynamics of DS. In the first case the mode $n = 0$ seems to be dominant, whereas in the second simulation series the mode $n = 1$ defines essentially the behavior of the system. From the other hand the interplay of both modes is obviously nontrivial, so one cannot speak about the "influence" of the one or another mode in the strict sense.

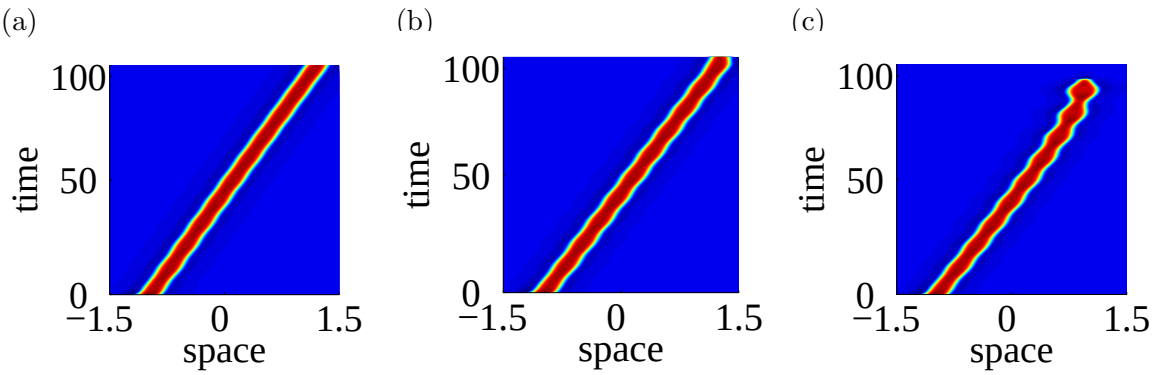

FIG. 7.18: Space-time plots of u for different values of θ obtained from numerical solution of (7.1) for $\tau = 0.9$. Time evolution of the cross-section of the initial pulse close to the stationary solution is shown; a) $\theta = 0.43$ moving and breathing DS. The velocity is constant, whereas the oscillation amplitude decreases; b) $\theta = 0.46$ moving with a constant velocity and breathing with a constant amplitude DS c) $\theta = 0.48$ DS moves with a constant velocity, whereas the amplitude of oscillation increases, what leads to the collapse of DS. Other parameters are the same as in Fig. 7.16.

7.5 Multimode destabilization of stationary DS

In this section we consider a more complicated situation. Namely, let us suppose that several modes become unstable and we are interested as before in the long-time dynamics of a single DS. Recall that the mode with $n = 0$ corresponds to the change of the size of the DS, $n = 1$ describes the shift of the solution and $n \geq 2$ corresponds to the different soliton's deformations. On the other hand Fig. 7.3 clearly indicates that for calculated values of the control parameters only first three critical modes are of interest. Therefore we have chosen control parameters τ and θ to be in region where the modes $n = 0$, $n = 1$ and $n = 2$ are unstable and we look for long time behavior of the initial pulse. The result is shown in Fig. 7.19. Initial pulse, close to the stationary DS starts to move. Because of instability of the modes with $n = 0$ and $n = 2$ the form of the moving soliton also changes (see Fig. 7.19 for $t = 10$). As is seen from Fig. 7.19 the radius of the moving soliton increases, and after some time the curved soliton forms a ring, as shown in Fig. 7.19 for $t = 34$. Finally the solution is represented by a spreading outward circular wave (see Fig. 7.19 for $t = 59$). Figure 7.20 shows another possible destabilization scenario. In this case initial pulse (Fig. 7.20 for $t = 0$) as well as in the previous case converges to curved front (Fig. 7.20 for $t = 10$), which curvature radius grows ($t = 32$), till the soliton forms a circular wave (a ring), as shown in Fig. 7.20 for $t = 46$. In contrast to the situation described above, here the overlapping endpoints of the solution give a rise to a new solitary pulse (see Fig. 7.20 for $t = 53$). The dynamics of the new pulse at the beginning is similar to the dynamics of the

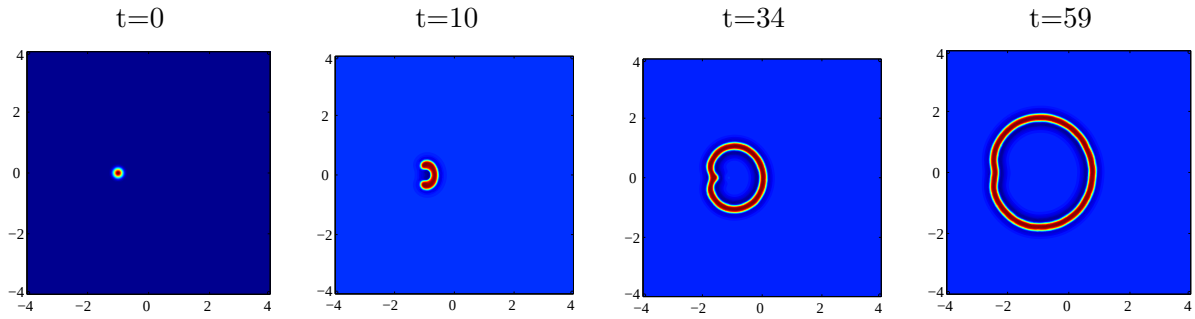

FIG. 7.19: Formation of the soliton ring from the initial distribution close to the stationary DS. Activator component u is depicted. Parameters: $D_u = 4.7 \cdot 10^{-3}$, $D_v = 0$, $D_w = 0.01$, $\lambda = 5.67$, $\kappa_1 = -1.04$, $\kappa_3 = 1.0$, $\kappa_4 = 3.33$, $\tau = 3$, $\theta = 0.01$.

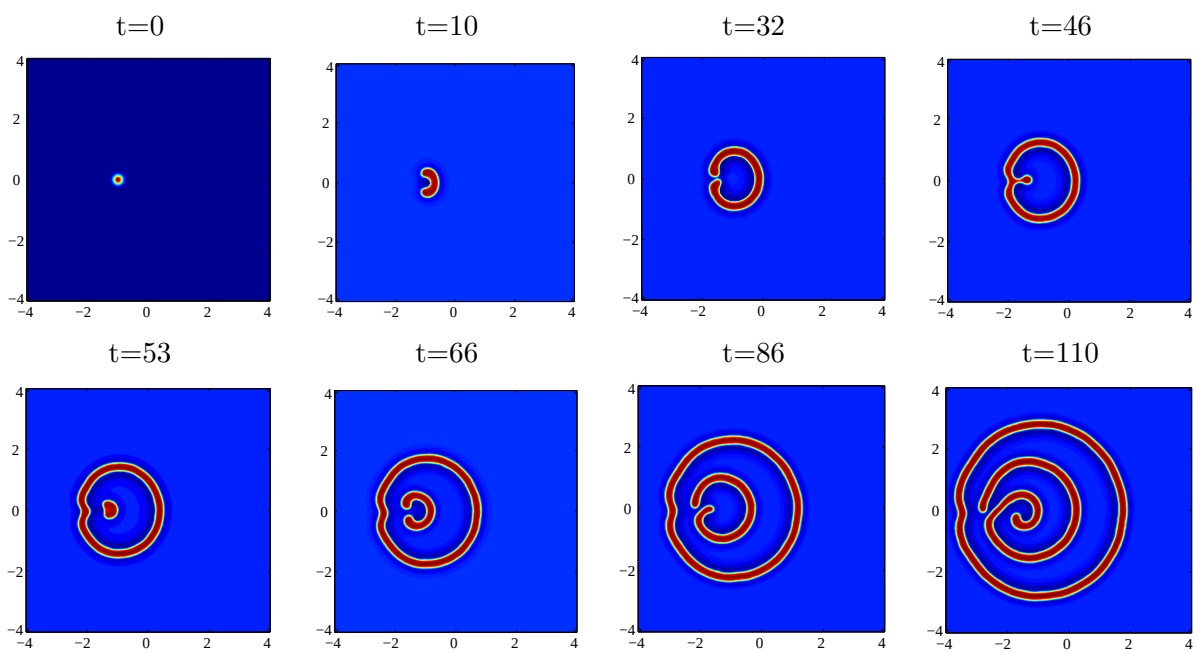

FIG. 7.20: Formation of the spiral-ring structure, formed from the stationary DS. The activator distribution u is to be seen. Parameters: $D_u = 4.7 \cdot 10^{-3}$, $D_v = 0$, $D_w = 0.01$, $\lambda = 5.67$, $\kappa_1 = -1.04$, $\kappa_3 = 1.0$, $\kappa_4 = 3.33$, $\tau = 14$, $\theta = 0.01$.

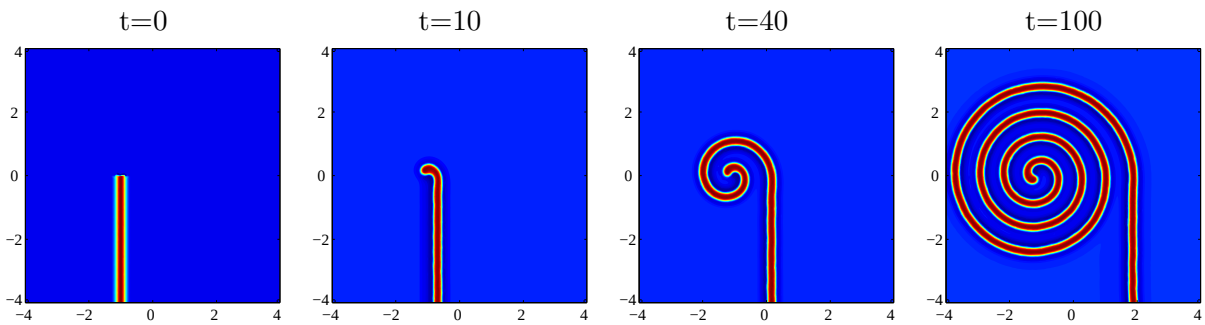

FIG. 7.21: Formation of the spiral. A half of a stripe is of use as an initial condition. The activator distribution u is depicted. Parameters: $D_u = 4.7 \cdot 10^{-3}$, $D_v = 0$, $D_w = 0.01$, $\lambda = 5.67$, $\kappa_1 = -1.04$, $\kappa_3 = 1.0$, $\kappa_4 = 3.33$, $\tau = 7$, $\theta = 0.01$.

first one ($t = 66$), however, the endpoints of the new pulse are not symmetrical, as can be seen in Fig. 7.20 for $t = 86$. Therefor the new pulse forms not a new ring, as before, but a spiral (Fig. 7.20 for $t = 110$). Note that if the endpoints of the new pulse would be symmetrical, a new ring could be formed instead of the spiral.

The mechanisms of structure formation, discussed above could be applied to the formation of some new structures, e.g., spirals. Indeed, let us choose the system parameters to be in the region where three first critical modes become unstable and consider a half of a stripe as an initial condition as shown in Fig. 7.21 for $t = 0$. Such an initial condition converges to the moving flat front, which curved free endpoint (see Fig. 7.21 for $t = 10$). The curved front proceeds the motion further and the endpoint forms the spiral, as shown in Fig. 7.21 for $t = 40$ and $t = 100$.

We conclude that an interplay between critical modes leads to formation of various stationary and dynamical structures, which can be described as a result of a long-time dynamics of a single stationary DS.